Approval of the Institute of Graduate Studies and Research

_____

Prof. Dr. Elvan Yılmaz
Director (a)

I certify that this thesis satisfies the requirements as a thesis for the degree of Master of Science in Mechanical Engineering.

_____

Assoc. Prof. Dr. Fuat Egelioğlu
Chair, Department of Mechanical Engineering

We certify that we have read this thesis and that in our opinion it is fully adequate in scope and quality as a thesis for the degree of Master of Science in Mechanical Engineering.

_____

Prof. Dr. Ibrahim Sezai
Supervisor

Examining Committee

_____

1. Prof. Dr. Ibrahim Sezai _____

2. Prof. Dr. Hikmet Aybar _____

3.Assoc. Prof. Dr. Fuat Egelioglu _____

Simulation of Melting of a Pure Substance Using Curvilinear Moving Grids

Amir Motaleb Mirlatifi

Submitted to the
Institute of Graduate Studies and Research
in partial fulfillment of the requirements for the Degree of

Master of Science
in
Mechanical Engineering

Eastern Mediterranean University
September 2009
Gazimağusa, North Cyprus

ABSTRACT

Melting and solidification of metals play an important role in material processing, metallurgy, welding, and growth of crystals from melts and solutions. There are generally two types of methods to simulate the melting/solidification processes: 1) The fixed grid methods 2) Moving grid methods. In the fixed grid approach a fixed grid is used in the real space of the problem and the solid-liquid interface is accounted for by using artificial source terms similar to the flow in porous media. In this method the interface position is not tracked but can be estimated indirectly and approximately. In the moving grid method the flow equations in the curvilinear moving plane are transformed into the fixed computational plane. Consequently, the solution of the transport equations as well as the position of the interface is tracked accurately. In this work Stefan condition is explained and mathematical modeling and numerical prediction of phase change processes of pure materials using curvilinear moving grids at macroscopic level is presented. The effectiveness of the method is demonstrated by adopting the conventional problem of Gallium melting. Grid refinement test is carried out and effects of different time steps as well as various Rayleigh and Stefan numbers are examined on the results.

ÖZET

Malzemelerin işlenmesi, metalurji ve eriyiklerle çözeltilerden kristal büyümesinde metallerin erime ve katılaşması önemli rol oynar. Erime/katılaşma işlemlerini simüle etmede genel olarak iki metod kullanılır: 1) Sabit grid metodu 2) Hareketli grid metodu. Sabit grid yaklaşımı kapsamında reel uzayda sabit bir grid kullanılır ve katı-sıvı geçişleri gözenekli ortamlardaki akışa benzer yapay kaynak terimleri kullanılarak çözümlenir. Bu metodda, katı-sıvı ara sınırı takip edilmez ama dolaylı yoldan ve yaklaşık olarak hesaplanabilir. Hareketli grid metodunda eğrisel uzaydaki akış denklemleri, sabit hesaplama düzlemine dönüştürülür. Sonuç olarak, taşıma denklemlerinin çözümü ve katı-sıvı ara sınırı kesin bir şekilde takip edilir. Bu çalışmada Stefan durumu açıklanmış ve eğrisel hareketli gridler makroskopik düzeyde kullanılarak saf malzemelerin hal değişim işlemlerinin matematiksel modellemesi ve sayısal tahmini yapılmıştır. Metodun etkililiği, geleneksel Galyumun erimesi problemine uyarlanarak denenmiştir. Grid iyileştirme testi yapılmış ve farklı zaman aralıkları, Rayleigh ve Stefan rakam değerleri kullanılarak sonuçta oluşan farklar gözlemlenmiştir.

ACKNOWLEDGEMENT

First and foremost I am deeply indebted to my supervisor Prof. Dr. Ibrahim Sezai without whom no thesis would have eventuated. His support, perpetual energy and enthusiasm in research, even throughout his holiday, has always been motivated me, and his knowledge has proved invaluable.

Prof. Hikmet Aybar and Dr. Fuat Egelioglu deserve special thanks as my thesis committee members and advisors.

My deepest gratitude goes to my family for their unflagging support and encouragement throughout my time at University.

Special thanks to Mr. Bariş Doğan for translating the abstract into Turkish.

At last but not the least, I offer my regards and blessings to the staff and academics of Eastern Mediterranean University, particularly those of Mechanical engineering and Industrial engineering departments, and all of those who supported me in any respect during the completion of the project.

This work is dedicated to my family for their continual support and forbearance

TABLE OF CONTENTS

LIST OF FIGURES

LIST OF TABLES

LIST OF SYMBOLS

A	Coefficients in the finite-difference equation
b	Source term
C_p	Specific heat (k J/ kg. K)
f	Pressure function
F	Face fluxes
g	Gravitational acceleration ($\mathrm{m/s^2}$), covariant matrix
$\sqrt{g}$	Jacobian of transformation
$\mathbf{g}_i$	covariant base vectors
$\mathbf{g}^i$	Contravariant base vectors
g_{ij}	Covariant metric tensor
g^{ij}	Contravariant metric tensor
H	Height (m)
h_{sf}	Latent heat (k J/kg)
k	Thermal conductivity (W/m. K)
L	Length (m)
P	Pressure (Pa)
Pr	Prandtl number, (ν/α)
q	Heat flux ($\mathrm{kW/m^2}$)
Ra	Rayleigh number $g\beta\Delta T L_{ref}^3/\nu\alpha$
S	Source term
St	Stefan number, $C_p\Delta T/h_{sf}$
T	Temperature (°C)

t	Time (Sec)
$\mathbf{u}$	Cartesian velocity vector
u, v	Velocity component in the Cartesian coordinate $(\mathrm{m/s})$
U, V	Contravariant velocities
V	Volume
x, y	Cartesian Coordinates

Greek symbols:

α	Thermal diffusivity $(\mathrm{m}^2/\mathrm{s})$
β	Volumetric thermal expansion coefficient $(1/\mathrm{K})$
ϕ	General variable, u, v, p, T
ν	Kinematic viscosity
μ	Dynamic viscosity $(\mathrm{kg.\,m/s})$
ρ	Density $(\mathrm{kg/m}^3)$
Γ	General diffusion coefficient
θ	Dimensionless temperature
ξ,η	Curvilinear coordinate

Subscripts:

c	Cold
cd	Cross derivative
e, w, n, s	CV cell faces
EE, E, W,	

WW, P, N, S	CV grid points
ne, se, we, ws	CV corner points
g	Grid
h	Hot
i	Solid or liquid
i, j	Cartesian coordinate
IN	Interface
l,s	Liquid, solid
m	Melting
ref	Reference
x,y	Differential with respect to x,y

Superscripts:

0	Previous time step
´	Differentiation, also correction term
$+, -$	Right, left
*	Indicates a quantity with dimension, also guessed values
$-$	Solid, liquid ratio
IN	Interface

COMMONLY USED ACRONYMS

CFD	Computational Fluid Dynamics
CV	Control Volume
MBP	Moving Boundary Problem
MIM	Momentum Interpolation Method
PDE	Partial Differential Equation
QUICK	Quadratic Upwind Interpolation for Convective Kinematics
SCL	Space Conservation Law
SIMPLE	Semi-Implicit Method for Pressure-Linked Equations
VOF	Volume of Fluid

CHAPTER 1

INTRODUCTION

1.1 State of Knowledge and Aim of Work

In the late 19th century, J. Stefan formulated the problem of finding the temperature distribution and freezing front history of a solidifying slab of water. From now on, the problem has been extended to include such complex phenomena as the solidification of alloy systems, supercooling, melting due to Joule heating and laser irradiation.

To the mathematician the Stefan problem is one which takes us slightly into the world of nonlinearity. Even if the PDEs that apply in the subdomains are linear, Stefan problems are, on the whole, nonlinear, and are even difficult to solve numerically.

To the computational scientist, modeling phase change processes need for advanced graphics and computing tools.

In the same vein, the engineer must struggle with complex technological challenges [1]. For instance, in some important parts of materials processing such as crystal growth, casting, welding, surface alloying, dip forming, spray coating and production of printed circuit electronics, phase changes of material are caused by the heat transfer to and from both of the phases on either side of the interface, which consequently solidification and melting occur [9].

Analytical solutions of the Stefan problem exist only for a small portion of cases. The well known analytical methods, Goodman's [11] and Neumann's methods [12] are merely used as a reference standard against which to validate the numerical methods. Resorting to numerical analysis is the only option for solving a more general equation. For example no analytical treatment of Stefan problem exists, when the convective terms are incorporated. Convection in the melt arises whenever the density of the liquid is not constant, and it is most notable when melting is induced by heating from below a liquid of relatively low viscosity. Often its primary effect is to enhance heat transfer (possibly by several orders of magnitude, in which case the liquid is effectively isothermal). Indeed, only a small proportion of the literature on Stefan-type problems deals with convection. This is of course mainly due to the serious mathematical and computational difficulties one encounters when dealing with convective flows.

The aim of the present work is mathematical modeling and numerical prediction of phase change processes of pure materials using moving grids at the macroscopic level. To do so, firstly fundamental background of the phenomena involved in the phase change and the Stefan condition is introduced. Secondly, the numerical methods applied to general moving boundary problems are given. Finally, the proposed numerical algorithm is investigated by applying it into a gallium melting problem.

1.2 Thesis organization

This thesis contains six chapters. A brief summary of the remaining five chapters are as follows.

Chapter 2 introduces the physics behind the phase change processes of melting and solidification. Subsequently, based on simplifying assumptions, one dimensional Stefan condition is obtained from the global heat balance and finally it is generalized to multiple dimensions.

In chapter 3 Lagrangian and Eulerian methods for solving the Stefan problem also known as moving boundary problem are described briefly and some existing techniques are introduced based on them. Governing equations in solid and liquid domains as well as the Stefan condition are presented and afterwards by using an appropriate normalization nondimensionalization is explained. Transformation of these equations and also their discretization are discussed. To deal with the grid skewness, grid sliding algorithm is mentioned. The final section devotes to the solution algorithm.

Chapter 4 is devoted to verification of the present code by the benchmark problem of the gallium melting in the cavity and the results are compared with the experimental results.

In chapter 5 special attention is paid to the interface evolution and flow structure in the melted gallium. One section attempts to resolve the controversy among the former researches for this problem. The problem is examined for two different time steps and grid independency test is presented for different number of grids and at various times. Effects of Rayleigh and Stefan numbers on the results are delineated and at last the change in physical volume is shown.

Chapter 6, as the conclusion, summarizes the numerical methodology and the results and emphasizes on the gird generation method and grid smoothing on the interface. Finally some recommendations are made for the future work.

CHAPTER 2

PHASE CHANGE FORMULATION

2.1 Introduction

This section concerned with simulating the phase change processes of melting and solidification on a macroscopic scale based on the classical Stefan-type model. This problem is nonlinear and its principal difficulty lies in the fact that one of its unknowns is the region in which it is to be solved. For this reason it is called a "moving boundary problem (MBP)." The formulation of MBPs requires not only the initial and boundary conditions to be known, as in boundary-value problems, but two more conditions are needed on the moving boundary; one to determine the boundary itself and the other to complete the definition of the solution of the differential equation. The differential equations of melting and solidification processes can be derived by imposing the continuity, momentum, and energy conservation within the liquid region, as well as the energy conservation in the solid domain, and a complementary condition expressing energy conservation, prevails along the curves separating solid from liquid. Despite of different curves shape for various materials, the classical formulation is based on an underlying assumption that the front is indeed of zero thickness.

In the following sessions, firstly an overview of the physics relevant to phase-change processes is discussed. Then, the precise mathematical formulation of the

basic physical facts leading to the “Stefan Problem”, the prototype of all phase-change models, is covered.

2.2 An Overview of the Phenomena Involved in a Phase Change

The principles, ideas, and many of the results from liquid-solid phase change, apply as well to other first-order phase transitions, including certain solid-to-solid, gas-liquid, and gas-solid transitions.

Solidification and melting involves several mechanisms such as heat (and often also mass) transfer, possible supercooling, absorption or release of latent heat, changes in thermophysical properties, surface effects, etc.

In a solid the molecules vibrate around fixed equilibrium positions, while in a liquid they may move freely between these positions. The macroscopic manifestation of this vibrational energy is what we call heat or thermal energy, the measure of which is temperature. Before a solid can melt it must acquire a certain amount of energy to overcome the binding forces that maintain its solid structure. This energy is referred to as the latent heat h_{sf} (heat of fusion) of the material and represents the difference in thermal energy (enthalpy) levels between liquid and solid states.

The transition from one phase to the other, that is, the absorption or release of the latent heat, occurs at some temperature. This phase change temperature (ex. T_m as melting temperature) depends on pressure and it may be considered constant under fixed pressure.

Since formation of a crystal may require the movement of atoms into the solid lattice structure, it is not infrequent that the temperature of the material is reduced below T_m without formation of solid. Thus supercooled liquid, which is a metastable state, may appear. Typical cooling curves for both normal freezing and supercooling

are shown schematically in Figure 2.1. Note that for the supercooling, provided that the latent heat of fusion is sufficient to raise the temperature up to the melt temperature T_m , crystallization does take place.

The phase-transition region where solid and liquid coexist is called the interface. For most pure materials solidifying under ordinary freezing conditions at a fixed T_m the interface appears (locally) planar and of negligible thickness. In other cases, typically resulting from supercooling, the phase transition region may have considerable thickness and is referred to as a "mushy zone"; its microstructure may now appear to be dendritic or columnar, Figure 2.2. The Gibbs-Thomson effect states that surface tension and interfacial curvature at a curved solid-liquid interface has influence on the local freezing temperature. It is small for the overall freezing process, yet affects the morphology of the interface from the microscopic point of view.

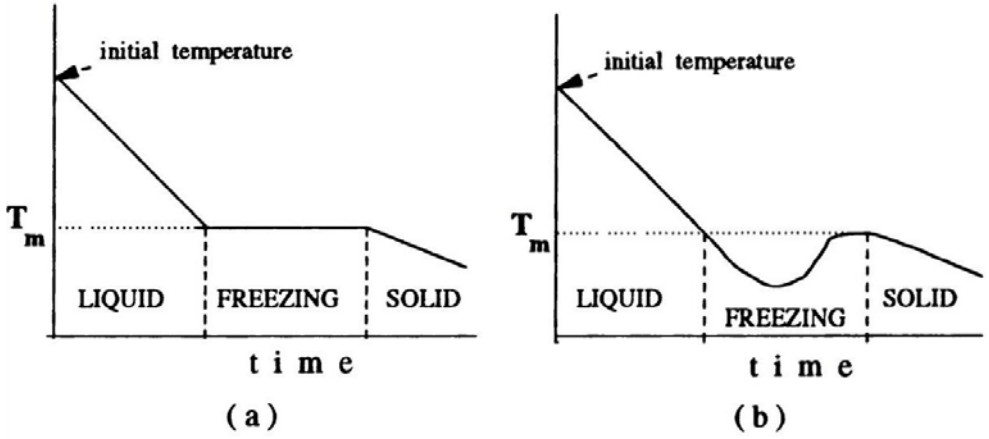

Figure 2.1: Cooling curves for (a) normal freezing and (b) supercooling, [1].

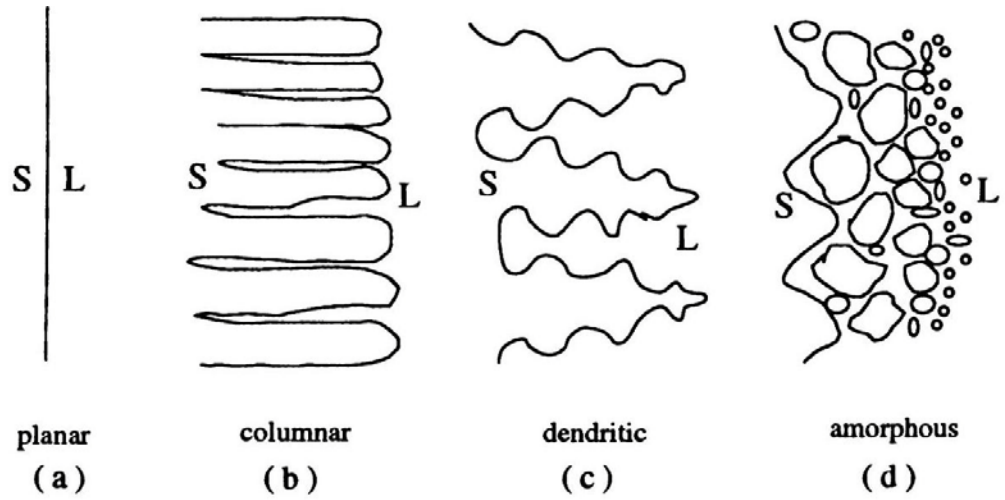

Figure 2.2: Schematic of Common Interfacial Morphologies, [1].

Although most thermophysical properties of a material are varying smoothly with temperature, sudden changes can be observed at T_m. Such discontinuities in thermophysical properties complicate the mathematical problems because they induce discontinuities in the coefficients of differential equations.

The aim of the present work is mathematical modeling and analysis of phase change processes at the macroscopic level. The purpose of mathematical modeling is to quantify the process in order to be able to predict (and ultimately control) the evolution of the temperature field in the material, the amount of energy used and stored, the interface location and thickness, and any other quantity of interest. Thus the equations and conditions that express the physics of the process must be formulated subject to certain accepted approximations

2.3 Assumptions

It is important to have a plain view of precisely which phenomena are taken into account and which are not. Assumptions in the following table simplify the

physical factors engaged in a phase change and they will lead us to the Stefan problem.

Table 2.1: Basic assumptions, [1].

Physical Factors Involved in phase change Processes	**Simplifying Assumptions for the Stefan Problem**	**Remarks on the Assumptions**
1. Heat and mass transfer by conduction, convection, radiation with possible gravitational, elastic, chemical and electromagnetic effects.	Heat transfer isotropically by conduction and convection only, all other effects except gravitational forces assumed negligible.	Most common case. Very reasonable for pure materials.
2. Release or absorption of latent heat	Latent heat is constant; it is released or absorbed at the phase-change temperature.	Very reasonable and consistent with the rest of the assumptions.
3. Variation of phase-change temperature	Phase-change temperature is a fixed known temperature, a property of the material.	Most common case, consistent with other assumptions.
4. Nucleation difficulties, supercooling effects	Assume not present.	Reasonable in many situations.
5. Interface thickness and structure	Assume locally planer and sharp (a surface separating the phases) at the phase-change temperature.	Reasonable for many pure materials (no internal heating present).
6. Surface tension and curvature effects at the interface	Assume insignificant.	Reasonable and consistent with other assumptions.
7. Variation of thermophysical properties	Assume constant in each phase, for simplicity ($C_{p,l} \neq C_{p,s},\ k_l \neq k_s$).	An assumption of convenience only. Reasonable for most materials under moderate temperature range variations. The significant aspect is their discontinuity across the interface, which is allowed.
8. Density changes	Assume constant ($\rho_l = \rho_s$).	Necessary assumption to avoid movement of material.

2.4 Formulation of Stefan Problem

As we mentioned earlier the Stefan Problem is a moving boundary problem; it requires an additional boundary condition to fix the position or motion of the boundary. In a heat transfer problem, one typically knows either the temperature or the heat flux at each point on the melting point of the material. Because the position of this boundary is unknown, however, we require another boundary condition to resolve its position and motion in time.

One-dimensional Stefan condition for pure materials can be obtained directly from an energy balance at the interface. Consider a slab of material of constant cross sectional area A, where $0 \leq x \leq l$. Heat is exchanging at faces $x = 0$ and $x = l$, resulting in a two-phase material with a sharp interface in between, see Figure 2.3.

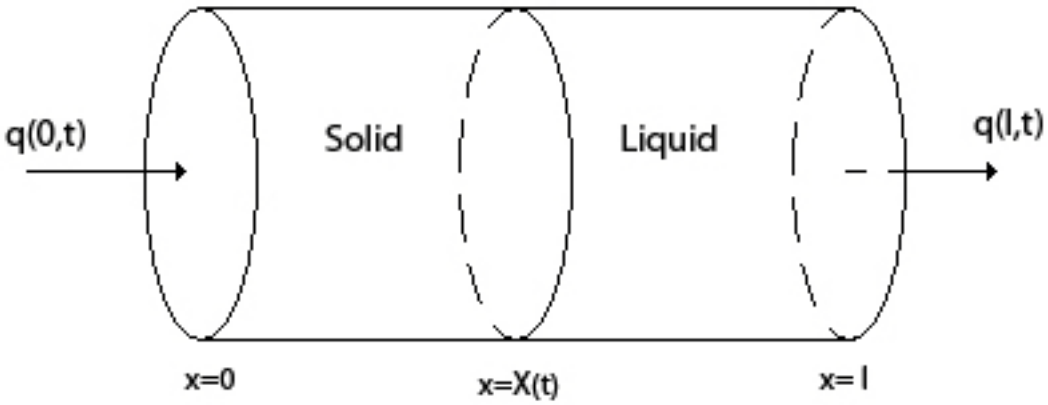

Figure 2.3: One-dimensional Phase-change Schematic.

Energy balance at the interface gives the one-dimensional Stefan condition as

$$\rho h_{sf} X^{'}(t) = k_S T_x(X(t)^{-}, t) - k_l T_x(X(t)^{+}, t) \tag{2.1}$$

where superscripts $+$ and $-$ refers to the right and left sides of the interface, respectively.

The Stefan condition can be generalized to multiple dimensions. In this case, we must account for the possibility that the interface is curved, in which case the area of the liquid-solid interface changes as the interface moves. By neglecting the surface energy effects, the Stefan condition is proved to be

$$\rho_s h_{sf} \mathbf{v}_{IN}^* = (k_s \nabla T_s - k_l \nabla T_l) \tag{2.2}$$

where $\mathbf{v}_{IN}^*$ stands for the interface velocity vector. This is the new boundary condition that is needed to account for the heat of fusion, and it completes the mathematical model. (For an inclusive account see reference [1]).

CHAPTER 3

NUMERICAL METHODS APPLIED TO GENERAL MOVING BOUNDARY PROBLEMS

3.1 Introduction

It is appropriate first to provide a brief survey of some existing techniques concerned with tracking highly distorted fronts in moving boundary problems. A variety of technique is available, each with its own strengths and weaknesses. The choice of an efficient and robust technique will depend on the physical problem under investigation. These techniques may be classified under two main categories:

- Surface tracking or moving domain (Lagrangian methods).
- Volume tracking or fixed-domain (Eulerian methods).

In the Lagrangian methods, the grid is configured to conform to the shape of the interface, and thus it adapts continually to it. The Eulerian methods employ a fixed grid formulation, and the interface between the two phases is not explicitly tracked but is reconstructed from the properties of appropriate field variables, such as fluid fractions.

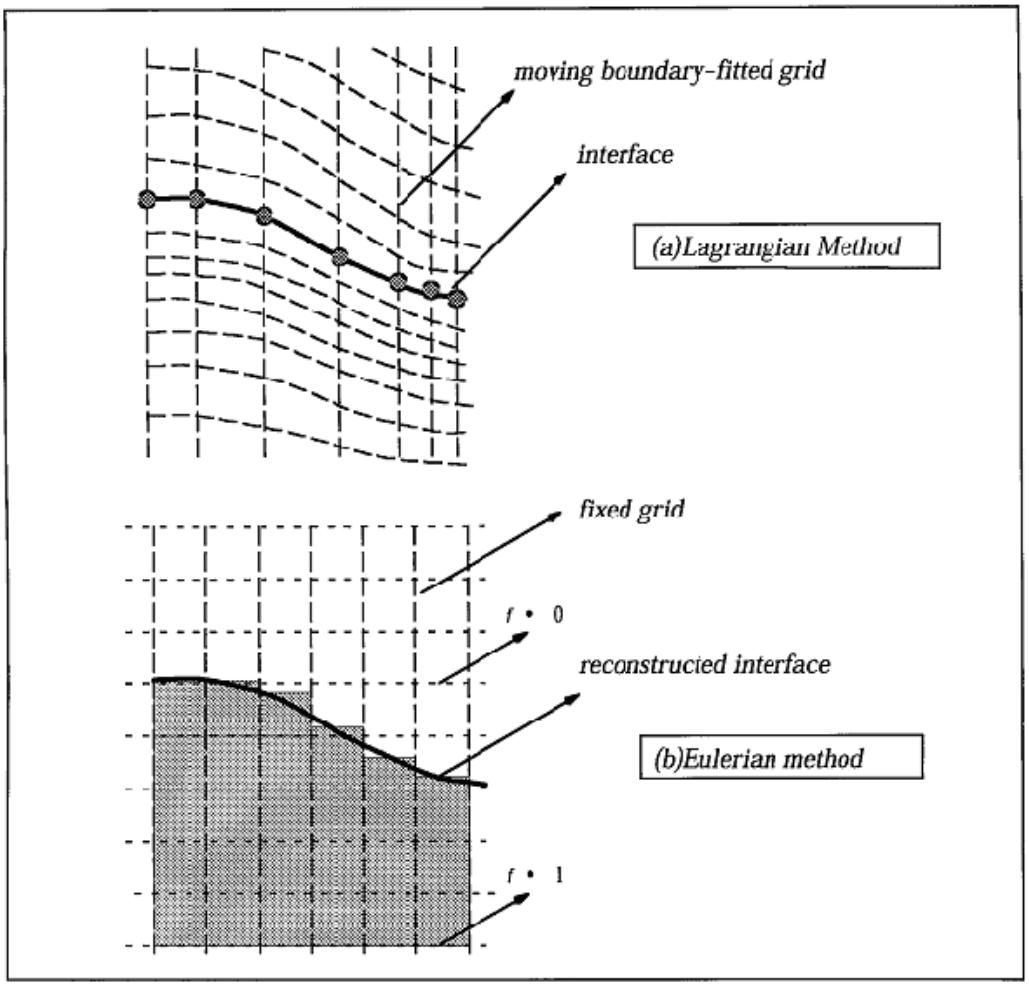

Figure 3.1: Lagrangian Methods vs. Eulerian Methods [3].

Based on these basic differences in approach of the two classes of methods, the following comparisons can be made:

3.1.1 Lagrangian vs. Eulerian Methods

Some features for Lagrangian methods are given in the following.

1. The interface considered as discontinuity which explicitly tracks its evolution. No modeling is necessary to define the interface. Hence, boundary conditions can be applied at the exact location of the interface.

2. Knowing the exact location of the interface the grid are fit to it. Therefore grid needs to be generated at each time. By advancing the interface with time the

grids may be skewed in the vicinity of the interface. In this regard, some methods have been developed to manipulate the grid skewness, such as the sliding grid algorithm used in [10].

We can characterize The Eulerian Methods as below

1. With the use of the volume fraction information or other equations, the interface location can be obtained approximately. Thus, boundary conditions are manipulated to appear in the governing transport equations.

2. The computation is performed on a fixed grid. However, when the interface is arbitrarily shaped very large number of grids are required to obtain accurate flow structure [29].

In general, lack of precise definition and details of the interface make Eulerian approach unsuitable for problems in which the interface configuration is of paramount importance. On the other hand, Lagrangian method encounters difficulties when the interface becomes multiple-valued or geometrically complicated. Hence, if details of the interface and flow features are of secondary importance, the Eulerian methods are more suitable, and if the discontinuity at the interface is managed with fidelity, Lagrangian methods hold an advantage.

Depending on the problem, numerical techniques with varying levels of complexity have to be developed. The level of sophistication desired is motivated by accuracy requirements in dealing with the interface, particularly if the interface shape becomes highly convoluted.

3.1.2 Review of Available Methods for Moving Boundary Problems

Under the broad categories of Lagrangian and Eulerian methods, a few techniques have been developed thus far by researchers in the area of moving boundary problems. Some of them are shown as follows.

3.1.2.1 Volume Tracking Methods

In this approach, the interface is not defined explicitly, or it is tracked but reconstructed at every step. The main difficulty arises in the reconstruction of the interface which involves a considerable number of logical operations. Volume-tracking methods have been applied to complex interfacial phenomena, including droplet dynamics and breakup, morphological instabilities in crystals and spray dynamics.

A special class of the fixed-domain formulation was first proposed by Voller et al. [2], which has gradually been developed by several authors, e.g. [4], [7]. In this approach, the total enthalpy, rather than the temperature, is considered as the primary dependent variable in the energy equation and, hence, a set of auxiliary relations is required between them.

Subsequent improvements in the enthalpy-porosity formulation resulted in an iterative updating of the liquid fraction, in consistency with the thermodynamics of the associated phase change process [8]. Irrespective of improvements, it has always been a difficult proposition to numerically simulate a sharp interface using enthalpy-porosity formulation primarily because of the limitations in using limitingly thin grid spacing near interfacial region. One inherent drawback of such techniques is that the temperature range over which the phase change is assumed to take place should be

set to zero (or, negligibly small) such that the formulation reduces to the classical Stefan problem [9].

In applications where only the broad features of interfacial behavior are required the VOF methods have been widely used, e.g. [13], [15]. The ability of this approach to accurately resolve an irregularly shaped interface needs to be improved.

3.1.2.2 The Level-Set Method

By using the level set method, highly distorted, and even three-dimensional interfaces have been obtained for solidification problems [16]. As with other purely Eulerian methods, topology changes are incorporated automatically. For highly nonequilibrium phenomena with arbitrary boundary conditions and inhomogeneous materials and convection in the melt, the applicability of the method needs further assessment. Moreover, the exact location of the interface does not automatically yield.

3.1.2.3 Phase Field Method

The phase field method has succeeded in generating realistic solidification microstructures [17]. The basic of the method lies in expressing the free energy of the system as a Cahn-Hilliard functional.

The solution of these equations leads to the development of realistic solidification patterns. The phase field model thus yields excellent qualitative results. However, in a general situation, the basis of the model is questionable [3]. Furthermore, it is difficult to correlate the several constants and parameters involved in the model to real physical systems. In addition, the interface is not explicitly tracked and one has to balance the need for an extremely fine grid resolution to

capture sharp interfaces with stability considerations for time-stepping. Thus, the phase field approach, while promising, cannot yet be regarded as a simulation technique for general solidification processes.

3.1.2.4 Body Fitted Coordinates Transformation

In this method, which is utilized in the present thesis, the irregular physical boundary is mapped by body-fitted, but structured meshes, on which the field equations are solved and moving boundaries tracked [3], [9]. As with most mapping methods, the calculations experience difficulties when the interface becomes multiple-valued. It is still possible to generate boundary-conforming grids beyond this stage, say by solving partial differential equations in each phase; however, the added expense of solving these equations is undesirable.

Boundary–fitted grids often experience difficulties in the form of grid skewness under severe interface convolution and need to be reconfigured under topological changes of the interface. Such events need to identified and dealt with- a process that will involve considerable logical and algorithmic complexity. Furthermore, the grid points and values of the field variables have to be redistributed in the vicinity of the interface, which may lead to additional numerical dissipation.

3.1.2.5 Lagrangian-Eulerian Methods

To combine the strengths of the moving grid and fixed grid techniques combined Lagrangian-Eulerian methods, in which a set of markers is employed to define and follow the interface in Lagrangian framework, is used. To facilitate the solution of the field equations, a fixed grid is utilized.

On the fixed grid system, the markers advance in time, causing the computational cells in the interface regions to become irregularly shaped. Special treatment is needed to enable accurate computations of the mass, momentum, and energy fluxes and to cast the discretized forms within a pressure-based, control volume framework.

This technique is dealt with sharp interface between the melt and the solid phases, as well as, large deformations of the interface.

3.2 Governing Equations and Solution Procedure

The major objective of this work is to demonstrate the correct modeling of phase change phenomena by using moving meshes and by satisfying the required space conservation law. We assume that the fluid is incompressible, laminar, and two-dimensional. Newtonian fluid is assumed for obtaining the general equations. The thermophysical properties are constant and uniform in various phases. Also, density is assumed constant during melting and solidification process. Yet, for the liquid case as long as changes in density are small, the Boussinesq approximation is applicable. At last, the viscous dissipation is considered as negligible.

Following the above assumptions, the two dimensional governing equations of the fields can be written in differential form as:

$$\frac{\partial u^*}{\partial x^*} + \frac{\partial v^*}{\partial y^*} = 0 \tag{3.1.a}$$

$$\frac{\partial u^*}{\partial t^*} + \frac{\partial (u^* u^*)}{\partial x^*} + \frac{\partial (u^* v^*)}{\partial y^*} = \frac{\mu}{\rho}\left(\frac{\partial^2 u^*}{\partial x^{*2}} + \frac{\partial^2 u^*}{\partial y^{*2}}\right) - \frac{1}{\rho}\frac{\partial P^*}{\partial x^*} \tag{3.1.b}$$

$$\frac{\partial v^*}{\partial t^*} + \frac{\partial (v^* u^*)}{\partial x^*} + \frac{\partial (v^* v^*)}{\partial y^*} = \frac{\mu}{\rho}\left(\frac{\partial^2 v^*}{\partial x^{*2}} + \frac{\partial^2 v^*}{\partial y^{*2}}\right) - \frac{1}{\rho}\frac{\partial P^*}{\partial y^*} - \beta(T - T_{ref})g \tag{3.1.c}$$

$$\frac{\partial T}{\partial t^*} + \frac{\partial (Tu^*)}{\partial x^*} + \frac{\partial (Tv^*)}{\partial y^*} = \frac{k_i}{\rho c_{p,i}} \left[\frac{\partial^2 T}{\partial x^{*2}} + \frac{\partial^2 T}{\partial y^{*2}} \right] \tag{3.1.d}$$

where asterisks represents the dimensional variables and T_{ref} is the reference temperature, which depends on the problem at hand. The term $-\beta(T - T_{ref})g$ derived from the Boussinesq approximation model in which the density treats as a constant value in all equations, except for the buoyancy term in the y-momentum equation. Subscript i in the energy equation (eqn.3.1.d) stands for l and s, which in turn represents the liquid and solid phases, respectively. It should be noted that for the solid phase, only the energy equation is solved, which can be obtained by neglecting the convective term at the left hand side of the equation (3.1.d).

As it is stated in chapter 2, the interface must move to satisfy local energy balance, which defines the interface position and motion as:

$$\rho h_{sf} \mathbf{v}_{\mathrm{IN}}^* = (k_s \nabla T_s - k_l \nabla T_l) \tag{3.2}$$

where $\mathbf{v}_{\mathrm{IN}}^*$ is the dimensional velocity vector of the interface, h_{sf} is the latent heat, and T is the dimensional temperature. Interface movement in any direction can be calculated by taking the appropriate dot product with eqn (3.2). For instance, in the Cartesian coordinates $\boldsymbol{i}$ and $\boldsymbol{j}$ are the unit vectors and $u_{IN}^* = (\mathbf{v}_{IN}^* . \boldsymbol{i})$ and $v_{IN}^* = (\mathbf{v}_{IN}^* . \boldsymbol{j})$ are the Cartesian components of the interface velocity vector. Hence we can write

$$\begin{aligned} \rho h_{sf} u_{\mathrm{IN}}^* &= (k_s \nabla T_s - k_l \nabla T_l).\mathbf{i} = k_s \frac{\partial T_s}{\partial x} - k_l \frac{\partial T_l}{\partial x} \\ \rho h_{sf} v_{\mathrm{IN}}^* &= (k_s \nabla T_s - k_l \nabla T_l).\mathbf{j} = k_s \frac{\partial T_s}{\partial y} - k_l \frac{\partial T_l}{\partial y} \end{aligned} \tag{3.3}$$

3.3 Dimensionless Form of Equations

Dealing with either dimensional or nondimensional variables is a matter of personal preference and there should be no real difference. However, experimental studies of flows are often carried out on models, and the results are displayed in dimensionless form, thus allowing scaling to real flow conditions. The same approach can be undertaken in numerical studies as well. The governing equations can be transformed to dimensionless form by using appropriate normalization. The following scales are used for nondimensionalization of the governing equations:

$$x = \frac{x^*}{L_{ref}}\ , y = \frac{y^*}{L_{ref}}\ , t = \frac{t^*}{\frac{L_{ref}}{u_{ref}}}\ , u = \frac{u^*}{u_{ref}}\ , v = \frac{v^*}{u_{ref}}$$

$$\theta = \frac{T - T_{ref}}{T_h - T_{ref}}, \qquad P = \frac{P^*}{\rho {U_{ref}}^2}, \qquad u_{ref} = \alpha_l / L_{ref} \tag{3.4}$$

where α_l is the thermal diffusivity of the liquid and T_h is typically the highest temperature in the system. T_{ref} is the reference temperature. For the present problem of Gallium melting (chapter 4), T_{ref} is chosen to be the temperature of the cold wall. Dimensionless forms of governing equations becomes:

$$\frac{\partial u}{\partial x} + \frac{\partial v}{\partial y} = 0 \tag{3.5.a}$$

$$\frac{\partial u}{\partial t} + \frac{\partial (uu)}{\partial x} + \frac{\partial (uv)}{\partial y} = Pr\left(\frac{\partial^2 u}{\partial x^2} + \frac{\partial^2 u}{\partial y^2}\right) - \frac{\partial P}{\partial x} \tag{3.5.b}$$

$$\frac{\partial v}{\partial t} + \frac{\partial (vu)}{\partial x} + \frac{\partial (vv)}{\partial y} = Pr\left(\frac{\partial^2 v}{\partial x^2} + \frac{\partial^2 v}{\partial y^2}\right) - \frac{\partial P}{\partial y} + Ra\ Pr\ \theta \tag{3.5.c}$$

$$\frac{\partial \theta}{\partial t} + \frac{\partial (\theta u)}{\partial x} + \frac{\partial (\theta v)}{\partial y} = \frac{\alpha_i}{\alpha_l}\left[\frac{\partial^2 \theta}{\partial x^2} + \frac{\partial^2 \theta}{\partial y^2}\right] \tag{3.5.d}$$

Once more i in equation (3.5.d) denotes l or s for the liquid and solid states, respectively. For the solid phase, the dimensionless energy equation can be obtained by ignoring the convective term in the equation (3.5.d).

Dimensionless Stefan condition at the interface can be written as:

$$\mathbf{v}_{IN} = Ste\left(\bar{k}\boldsymbol{\nabla}\theta_s - \boldsymbol{\nabla}\theta_l\right) \tag{3.6}$$

where $\mathbf{v}_{IN}$ is the nondimensional interface velocity vector $\mathbf{v}_{IN} = \mathbf{v}_{IN}^{*}/u_{ref}$, and $\bar{k} = k_s/k_l$.

The above nondimensionalization gives rise to the following nondimensional numbers that characterize most of the problems:

Rayleigh number: $Ra = g\beta\Delta T{L_{ref}}^3/\nu\alpha$ (3.7.a)

Prandtl number: $Pr = \frac{\upsilon}{\alpha} = \frac{c_{p,l}\mu}{k}$ (3.7.b)

Stefan number: $Ste = c_{p,l}\Delta T/h_{sf}$ (3.7.c)

Thermal diffusivities: $\alpha_l = \frac{k_l}{\rho c_{p,l}}$, $\alpha_s = \frac{k_s}{\rho c_{p,s}}$ (3.7.d)

h_{sf} is the latent heat of fusion, and ΔT is the temperature difference. For Gallium melting (chapter 4), ΔT is chosen to be $(T_h - T_c)$.

3.4. Grids with appropriate Transformations

In finite volume approach calculations requires to be made over a collection of discrete grid points. The arrangement of these discrete points throughout the flow field is simply called a grid. The way that such a grid is determined is called grid generation. The type of grid you choose for a given problem can make or break the numerical solution.

In most real problems such as solidification and melting, the rectangular grid is not appropriate for the solution of the flow field. Instead, a non-uniform, curvilinear

grid is required in order for the grid points to fall on the surface of the interface and boundaries. New coordinate lines ξ and η are defined such that the interface becomes a coordinate line, $\xi =$ constant, Figure 3.2. This is called a boundary-fitted coordinate system, where grid points automatically fall on the interface surface.

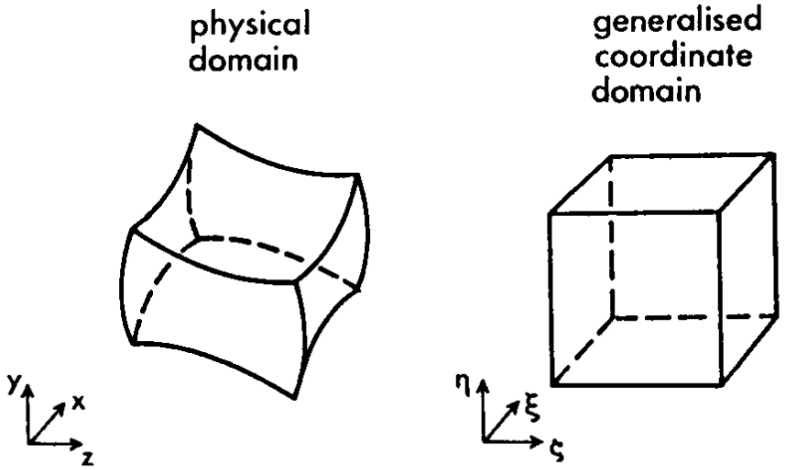

Figure 3.2: Transformation from physical domain to computational domain [21].

The generation of an appropriate grid or mesh is one thing; the solution of the governing flow equations over such a grid is quite another thing [6]. The standard finite volume approach requires a uniform grid. We do not have a direct way of numerically solving the governing flow equations over a nonuniform grid within the context of a finite volume method, for the conventional difference quotients are impossible to use. Instead, the non-uniform grid in physical space (fig. 3.3.a) must be transformed into a uniform, rectangular grid in terms of ξ and η (fig. 3.3.b). Moreover, along with this transformation, the governing partial differential equations must be recast so as to apply in this transformed, rectangular grid.

The rectangular grid shown in fig. 3.3.b is called the computational plane. The transformation must be defined such that there is one-to-one correspondence between the rectangular grid in Fig. 3.3.b and the curvilinear grid in Fig. 3.3.a, called

the physical plane. For instance, points a, b, and c in the physical plane (Fig 3.3.a) correspond to points a, b, and c in the computational plane, which involves uniform $\Delta\xi$ and uniform $\Delta\eta$. The governing partial differential equations are solved by a finite-volume method carried out in the computational space (Fig 3.3.b). Then the computed information is directly carried back to the physical plane via the one-to-one correspondence of grid points. Moreover, when the governing equations are solved in the computational space, they must be expressed in terms of the variables ξ and η rather than of x and y. That is, the governing equations must be transformed from (x, y) to (ξ, η) as the new independent variables.

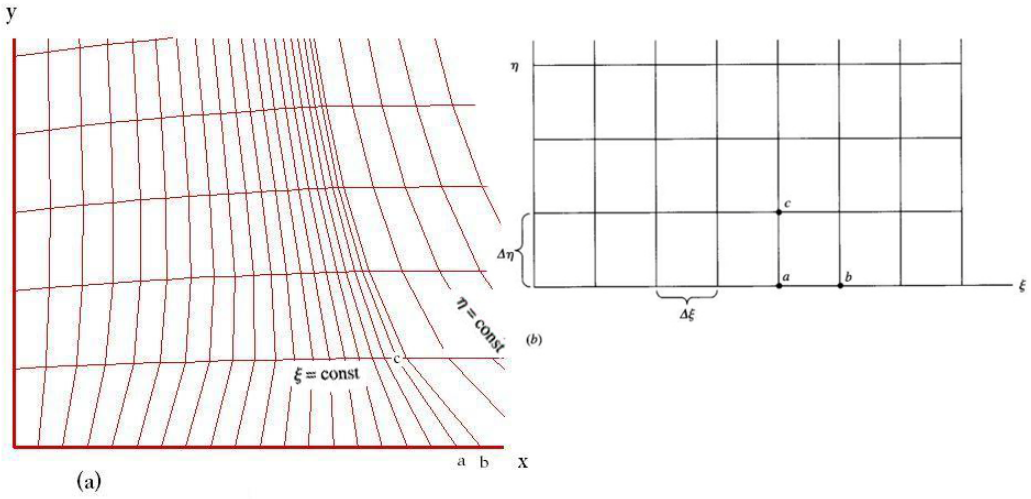

Figure 3.3: Schematic of a boundary fitted coordinate system. (a) Physical Plane; (b) computational Plane [6].

3.5 The Transformed Version of the Governing Equations

The purpose of this section is to describe the general transformation of the governing partial differential equations between the physical plane and the computational plane.

The use of a generalized coordinate implies that a deformed region in physical space will be mapped to a regular, rectangular region in computational space[21]. Accordingly, all computations are performed in the transformed space where the grid mesh is uniform and Cartesian. Consequently, techniques appropriate for standard Cartesian models can be applied directly without modification [20]. However, since one must pay close attention to how the transformation metrics are discretized, this simplicity does not come without a price. For the sake of brevity, development of the transformation relations which are required to derive the transformed version of governing equation are summarized here and the reader is recommended to consult to references (e.g. [19],[20]).

For two-dimensional situations in which field variables depend on the rectangular Cartesian coordinates x and y, covariant base vectors, $\mathbf{g}_1$ and $\mathbf{g}_2$ are

$$\mathbf{g}_1 = \boldsymbol{i}x_\xi + \boldsymbol{j}y_\xi \quad , \quad \mathbf{g}_2 = \boldsymbol{i}x_\eta + \boldsymbol{j}y_\eta, \tag{3.8}$$

where suffixes denote partial differentiation, e.g. $x_\xi = \partial x/\partial \xi$. Given the set $\{\mathbf{g}_1, \mathbf{g}_2\}$ we can form the set of contravariant base vectors, $\{\mathbf{g}^1, \mathbf{g}^2\}$ defined by the set of scalar product identities, (see Figure 3.4).

$$\mathbf{g}^i . \mathbf{g}^j = \delta_j^i \tag{3.9}$$

where δ_j^i is the kronecker symbol given by

$$\delta_j^i = \begin{cases} 1 & when\ i = j \\ 0 & when\ i \neq j \end{cases} \tag{3.10}$$

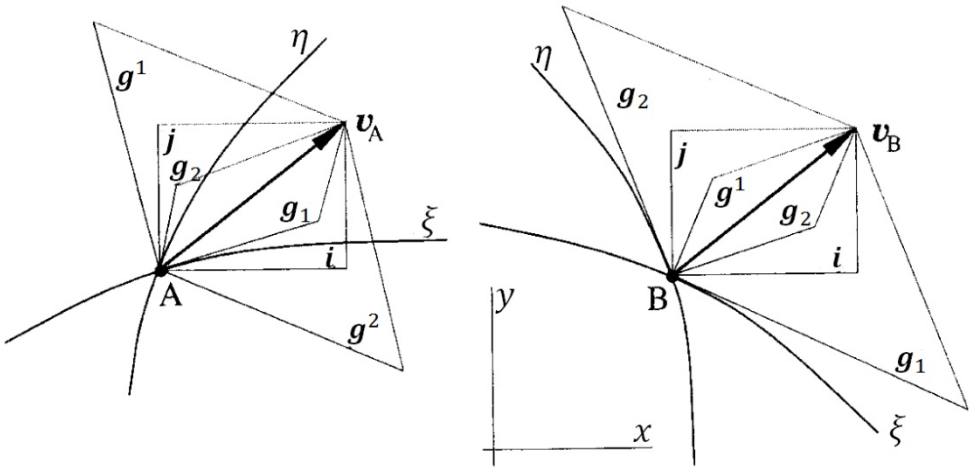

Figure 3.4: Cartesian, Contravariant, and covariant directions [$v_A = v_B$].

Contravariant base vectors can be written as

$$\mathbf{g}^1 = \boldsymbol{i}\xi_x + \boldsymbol{j}\xi_y \quad , \quad \mathbf{g}^2 = \boldsymbol{i}\eta_x + \boldsymbol{j}\eta_y \tag{3.11.a}$$

or

$$\mathbf{g}^1 = \frac{1}{\sqrt{g}}\left(\boldsymbol{i}y_\eta - \boldsymbol{j}x_\eta\right) \quad , \quad \mathbf{g}^2 = \frac{1}{\sqrt{g}}\left(-\boldsymbol{i}y_\xi + \boldsymbol{j}x_\xi\right) \tag{3.11.b}$$

Given a set of curvilinear coordinates $\{\xi, \eta\}$ with covariant base vectors $\mathbf{g}_i$ and contravariant base vectors $\mathbf{g}^i$, we can define the covariant and contravariant metric tensors respectively as the scalar products

$$g_{ij} = \mathbf{g}_i . \mathbf{g}_j \tag{3.12.a}$$

$$g^{ij} = \mathbf{g}^i . \mathbf{g}^j , \tag{3.12.b}$$

where i and j are 1 or 2 in two dimensions. The components of the covariant metric tensor are given by

$$g_{11} = x_\xi^2 + y_\xi^2 \tag{3.13.a}$$

$$g_{22} = x_\eta^2 + y_\eta^2 \tag{3.13.b}$$

$$\mathrm{g}_{12} = \mathrm{g}_{21} = x_\xi x_\eta + y_\xi y_\eta \tag{3.13.c}$$

Formulas for g^{ij} are, similarly, can be written as

$$g^{11} = \frac{g_{22}}{g} = \frac{{x_\eta}^2 + {y_\eta}^2}{g} \tag{3.14.a}$$

$$g^{22} = \frac{g_{11}}{g} = \frac{{x_\xi}^2 + {y_\xi}^2}{g} \tag{3.14.b}$$

$$g^{12} = g^{21} = \frac{-g_{12}}{g} = -\frac{x_\xi x_\eta + y_\xi y_\eta}{g} \tag{3.14.c}$$

From the properties of determinants it also follows that

$$g = \det(g_{ij}) = V^2 = g_{11}g_{22} - {g_{12}}^2 \tag{3.15.a}$$

and

$$V = \sqrt{g} = (x_\xi y_\eta - x_\eta y_\xi) \tag{3.15.b}$$

where V represents the volume formed between the covariant base vectors. Two-dimensional conservative forms of Gradient, Divergence, Laplacian operators are:

$$\nabla\varphi = \frac{1}{\sqrt{g}}\left\{\frac{\partial}{\partial\xi}\left(\sqrt{g}\mathbf{g}^1\varphi\right) + \frac{\partial}{\partial\eta}\left(\sqrt{g}\mathbf{g}^2\varphi\right)\right\} \tag{3.16.a}$$

$$\nabla.\mathbf{u} = \frac{1}{\sqrt{g}}\left\{\frac{\partial}{\partial\xi}\left(\sqrt{g}\mathbf{g}^1.\mathbf{u}\right) + \frac{\partial}{\partial\eta}\left(\sqrt{g}\mathbf{g}^2.\mathbf{u}\right)\right\} \tag{3.16.b}$$

$$\begin{aligned}\nabla^2\phi &= \nabla.(\nabla\phi)\\ &= \frac{1}{\sqrt{g}}\left\{\frac{\partial^2}{\partial\xi^2}\left(\frac{g_{22}}{\sqrt{g}}\phi\right) - \frac{\partial^2}{\partial\xi\partial\eta}\left(\frac{g_{12}}{\sqrt{g}}\phi\right)\right.\\ &\left. + \frac{\partial^2}{\partial\eta^2}\left(\frac{g_{11}}{\sqrt{g}}\phi\right) - \frac{\partial}{\partial\xi}[(\sqrt{g}\nabla^2\xi)\phi] - \frac{\partial}{\partial\eta}[(\sqrt{g}\nabla^2\eta)\phi]\right\}\end{aligned} \tag{3.16.c}$$

where $\mathbf{u} = u\boldsymbol{i} + v\boldsymbol{j}$.

Furthermore, the time derivative of the quantity ϕ at a fixed point of the physical domain (i.e. x and y) is related to its time-derivative at a fixed point of the computational domain (i.e. ξ and η) by the equation

$$\left(\frac{\partial \phi}{\partial t}\right)_{x,y} = \left(\frac{\partial \phi}{\partial t}\right)_{\xi,\eta} - \mathbf{u}_g . \nabla \phi \tag{3.17}$$

where subscripts outside the brackets indicate which variables are being held constant when partial differentiation is performed, and

$$\mathbf{u}_g = \left(\frac{\partial \mathbf{r}}{\partial t}\right)_{\xi,\eta} \tag{3.18}$$

is the rate of change of position of a given grid point in the physical domain, and $\nabla \phi$ evaluated in the physical domain.

Conserved form of all the operators, equations (3.16.a-c), in terms of contravariant variables are applied into the strong conservation form of the governing equations. Thus, we are able to retain in our transformed space all those advantages of the strong conservation form. Using the Cartesian velocity components rather than the contravariant components in the resulting governing equations can lead us to the transformed version of the governing equations. For the two dimensional case, the transformed relations of conservation laws are as follows

3.5.1 Continuity equation

Here, for the sake of clarity, the continuity equation is transformed to a time-dependent curvilinear coordinate system ξ and η. Other transport equations follow the same process and only the results are presented. Compressible continuity equation can be written in terms of the density function $\rho(x, y, t)$as

$$\left(\frac{\partial \rho}{\partial t}\right)_{x,y} + \nabla . (\mathbf{v}\rho) = 0. \tag{3.19}$$

From eqn. (3.17) we have immediately

$$\left(\frac{\partial \rho}{\partial t}\right)_{\xi,\eta} - \mathbf{u}_g . \nabla \rho + \nabla . (\mathbf{v}\rho) = \left(\frac{\partial \rho}{\partial t}\right)_{\xi,\eta} + \rho \nabla . \mathbf{u}_g + \nabla . \left[(\mathbf{v} - \mathbf{u}_g)\rho\right] = 0 \tag{3.20}$$

where $\mathbf{u}_g$ is the rate of change of position of a given grid point in the physical domain and is called the grid point velocity (eqn 3.18). By using (3.16) and after some rearrangement we can write

$$\frac{\partial}{\partial t}\left(\sqrt{g}\rho\right)+\frac{\partial}{\partial \xi}\left[\rho\sqrt{g}\mathbf{g}^1.\left(u-u_g\right)\boldsymbol{i}\right]+\frac{\partial}{\partial \eta}\left[\rho\sqrt{g}\mathbf{g}^2.\left(v-v_g\right)\boldsymbol{j}\right]=0 \tag{3.21}$$

For an incompressible fluid ρ is constant and it is eliminated from eqn (3.21). By using eqn (3.11.b) and (3.21) we can rewrite the continuity equation as

$$\frac{\partial\left(\sqrt{g}\right)}{\partial t}+\frac{\partial(U)}{\partial \xi}+\frac{\partial(V)}{\partial \eta}=0 \tag{3.22}$$

where U and V are contravariant velocities and can be defined by

$$U=y_\eta\left(u-u_g\right)-x_\eta\left(v-v_g\right) \tag{3.23}$$

$$V=-y_\xi\left(u-u_g\right)+x_\xi\left(v-v_g\right)$$

Note that the dimensionless governing equations are to be solved, and accordingly u_g and v_g are dimensionless Cartesian grid velocities. That is

$$\left(u_g,v_g\right)=\left({u_g}^*,{v_g}^*\right)/u_{ref} \tag{3.24}$$

3.5.2 X-Momentum equation

$$\begin{aligned}\frac{\partial\left(\sqrt{g}u\right)}{\partial t}+\frac{\partial(uU)}{\partial \xi}+\frac{\partial(uV)}{\partial \eta}&\\ =\Pr\left\{\frac{\partial}{\partial \xi}\left[\sqrt{g}\left(g^{11}\frac{\partial u}{\partial \xi}+g^{12}\frac{\partial v}{\partial \eta}\right)\right]\right.&\\ \left.+\frac{\partial}{\partial \eta}\left[\sqrt{g}\left(g^{22}\frac{\partial u}{\partial \eta}+g^{21}\frac{\partial u}{\partial \xi}\right)\right]\right\}-f(P)&\end{aligned} \tag{3.25}$$

3.5.3 Y-momentum equation

$$\frac{\partial\left(\sqrt{g}v\right)}{\partial t}+\frac{\partial(vU)}{\partial\xi}+\frac{\partial(vV)}{\partial\eta}$$
$$=\Pr\left\{\frac{\partial}{\partial\xi}\left[\sqrt{g}\left(g^{11}\frac{\partial v}{\partial\xi}+g^{12}\frac{\partial v}{\partial\eta}\right)\right]\right.$$
$$\left.+\frac{\partial}{\partial\eta}\left[\sqrt{g}\left(g^{22}\frac{\partial v}{\partial\eta}+g^{21}\frac{\partial v}{\partial\xi}\right)\right]\right\}-f(P)$$
$$+\sqrt{g}\,Ra\,\Pr\theta \tag{3.26}$$

where

$$f(P)=\frac{\partial(y_\eta P)}{\partial\xi}+\frac{\partial(-y_\xi P)}{\partial\eta}\qquad\text{for x-momentum}$$
$$f(P)=\frac{\partial(-x_\eta P)}{\partial\xi}+\frac{\partial(x_\xi P)}{\partial\eta}\qquad\text{for y-momentum} \tag{3.27}$$

3.5.4 Energy Equation for Liquid Phase

$$\frac{\partial\left(\sqrt{g}\theta\right)}{\partial t}+\frac{\partial(U\theta)}{\partial\xi}+\frac{\partial(V\theta)}{\partial\eta}$$
$$=\left\{\frac{\partial}{\partial\xi}\left[\sqrt{g}\left(g^{11}\frac{\partial\theta}{\partial\xi}+g^{12}\frac{\partial\theta}{\partial\eta}\right)\right]\right.$$
$$\left.+\frac{\partial}{\partial\eta}\left[\sqrt{g}\left(g^{22}\frac{\partial\theta}{\partial\eta}+g^{21}\frac{\partial\theta}{\partial\xi}\right)\right]\right\} \tag{3.28}$$

3.5.5 Energy Equation for Solid Phase

$$\frac{\partial\left(\sqrt{g}\theta\right)}{\partial t}+\frac{\partial(U\theta)}{\partial\xi}+\frac{\partial(V\theta)}{\partial\eta}$$
$$=\frac{\alpha_S}{\alpha_l}\left\{\frac{\partial}{\partial\xi}\left[\sqrt{g}\left(g^{11}\frac{\partial\theta}{\partial\xi}+g^{12}\frac{\partial\theta}{\partial\eta}\right)\right]\right.$$
$$\left.+\frac{\partial}{\partial\eta}\left[\sqrt{g}\left(g^{22}\frac{\partial\theta}{\partial\eta}+g^{21}\frac{\partial\theta}{\partial\xi}\right)\right]\right\} \tag{3.29}$$

In equation (3.29) the contravariant velocities (U and V) are calculated from eqn (3.23), by setting velocity field (u and v) to zero; So, merely the grid movement is considered.

3.5.6 Space Conservation Law (SCL)

In solidification and melting problems the solution domain changes in time due to the movement of the S/L interface, which must be calculated as part of the solution. Accordingly, the grids in the whole domain have to move with the interface. When cell faces move, the conservation of mass (and all other conserved quantities) is not necessarily ensured if the grid velocities are used to calculate the mass fluxes, and the problem of artificial mass sources arises.

Mass conservation can be obtained by enforcing the so-called space conservation law (SCL) or the conservation of the volume. Hence, Demirdzic´ and Peric´ [18] and Shyy [3] have shown in different ways that in addition to the conservation equations for physical quantities, such as mass, momentum and energy, an additional space conservation law has to be satisfied in order to avoid the inclusion of an artificial mass source (or sink) in the continuity equation. The differential version of this equation can be found by setting the velocity field in the continuity equation, eqn (3.18), to zero. i.e.:

$$\frac{\partial(\sqrt{g})}{\partial t} + \frac{\partial(U_g)}{\partial \xi} + \frac{\partial(V_g)}{\partial \eta} = 0 \tag{3.30}$$

where U_g and V_g are the contravariant fluxes appeared as a result of grid movement.

$$\begin{aligned} U_g &= y_\eta u_g - x_\eta v_g \\ V_g &= -y_\xi u_g + x_\xi v_g \end{aligned} \tag{3.31}$$

u_g and v_g are the Cartesian velocities of the cell faces due to grid movement.

3.5.7 Stefan Condition

For the Stefan equation, non-conservative representation of the gradient operator in general curvilinear coordinates is utilized.

$$\nabla\theta = (\mathbf{g}^1 \frac{\partial\theta}{\partial\xi} + \mathbf{g}^2 \frac{\partial\theta}{\partial\eta}) \tag{3.32}$$

By substitution of this equation and eqn (3.16.b) into eqn (3.6) the Stefan equation leads to

$$\begin{aligned} u_{IN} &= \mathrm{Ste}\left\{\frac{\bar{k}}{\sqrt{g}}\left[y_\eta \frac{\partial\theta_s}{\partial\xi} - y_\xi \frac{\partial\theta_s}{\partial\eta}\right] - \frac{1}{\sqrt{g}}\left[y_\eta \frac{\partial\theta_l}{\partial\xi} - y_\xi \frac{\partial\theta_l}{\partial\eta}\right]\right\} \\ v_{IN} &= \mathrm{Ste}\left\{\frac{\bar{k}}{\sqrt{g}}\left[-x_\eta \frac{\partial\theta_s}{\partial\xi} + x_\xi \frac{\partial\theta_s}{\partial\eta}\right] - \frac{1}{\sqrt{g}}\left[-x_\eta \frac{\partial\theta_l}{\partial\xi} + x_\xi \frac{\partial\theta_l}{\partial\eta}\right]\right\} \end{aligned} \tag{3.33}$$

where u_{IN} and v_{IN} are Cartesian components of the dimensionless velocity of the interface, and they can be easily related with the dimensional velocities of the interface in equation (3.3) by

$$(u_{IN}, v_{IN}) = (u_{IN}^*, v_{IN}^*)/u_{ref} \tag{3.34}$$

We should emphasize that the nonconservative form of the Stefan condition was failed to exhibit the true outcome.

3.5.8 Summary

The transport equations (3.22), (3.25), (3.26), (3.28), and (3.29) can be summarized in a general form as follows

$$\frac{\partial\left(\sqrt{g}\phi\right)}{\partial t}+\frac{\partial(\phi U)}{\partial \xi}+\frac{\partial(\phi V)}{\partial \eta}$$

$$=\Gamma\left\{\frac{\partial}{\partial \xi}\left[\sqrt{g}\left(g^{11}\frac{\partial \phi}{\partial \xi}+g^{12}\frac{\partial \phi}{\partial \eta}\right)\right]\right. \tag{3.35}$$

$$\left.+\frac{\partial}{\partial \eta}\left[\sqrt{g}\left(g^{22}\frac{\partial \phi}{\partial \eta}+g^{21}\frac{\partial \phi}{\partial \xi}\right)\right]\right\}-f(P)+\sqrt{g}S_{\phi}$$

where

Table 3.1: General form of the governing equations.

	ϕ	Γ	$f(P)$	S_{ϕ}
Continuity	1	0	0	0
X-momentum	u	Pr	$\frac{\partial}{\partial \xi}\left(y_{\eta}P\right)+\partial/\partial\eta(-y_{\xi}P)$	0
y-momentum	v	Pr	$\frac{\partial}{\partial \xi}\left(-x_{\eta}P\right)+\partial/\partial\eta(x_{\xi}P)$	$Ra\ Pr\ \theta$
Energy(liquid)	θ	1	0	0
Energy(solid)	θ	α_S/α_l	0	0

and contravariant velocities U and V can be found by eqn (3.23) in which for the solid region u and v velocities are set to zero.

The space conservation law is presented by equation (3.30) and Cartesian components of the interface velocities are found by (3.33).

3.6 Discretization

As we mentioned in the previous section, in the case of moving grids, the volume and the surface area of the control volume are not constant in time. Therefore, we performed the coordinate transformation into an orthogonal and fixed plane. As a result, the equations were written in curvilinear form. Now the finite volume method is used to discretize these governing equations. A collocated grid system in which all variables are stored at the center of the control volume in the computational plane is used (Figure 3.5).

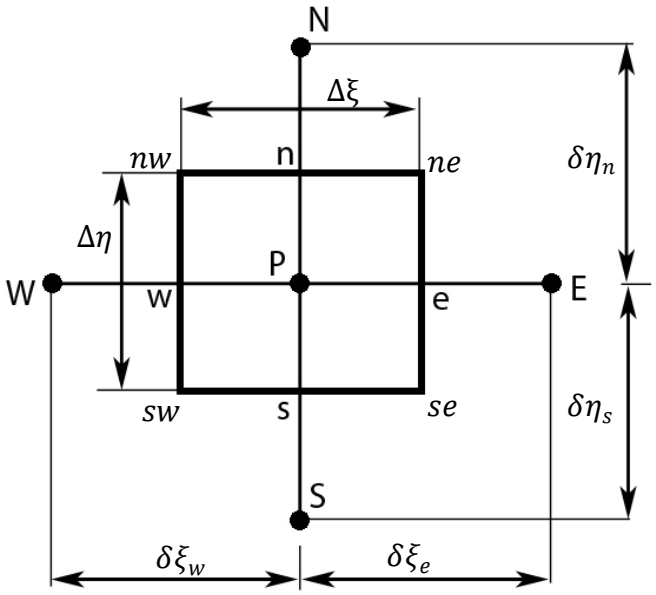

Figure 3.5: Collocated grid arrangement in the computational plane.

Using a first order fully implicit time integration, as well as the midpoint approximation rule for the surface and volume integrals of the general transport equation in the curvilinear form, eqn (3.35), with bounded cell faces $e, w, n,$ and s surrounding center P, leads to

$$\frac{\sqrt{g}\phi_P - \left(\sqrt{g}\phi_P\right)^0}{\Delta t}\Delta\xi\Delta\eta + \left([U\phi]_w^e \Delta\eta + [V\phi]_s^n \Delta\xi\right)$$

$$= \Gamma\left(\sqrt{g}g^{11}\frac{\partial\phi}{\partial\xi}\right)_w^e \Delta\eta + \Gamma\left(\sqrt{g}g^{22}\frac{\partial\phi}{\partial\eta}\right)_s^n \Delta\xi$$

$$+ \Gamma\left(\sqrt{g}g^{12}\frac{\partial\phi}{\partial\eta}\right)_w^e \Delta\eta - \Gamma\left(\sqrt{g}g^{12}\frac{\partial\phi}{\partial\xi}\right)_s^n \Delta\xi - f(P)\Delta\xi\Delta\eta \quad (3.36)$$

$$+ \sqrt{g}S\phi\ \Delta\xi\Delta\eta$$

where

$$f(P) = \left[\left(y_\eta P\right)_w - \left(y_\eta P\right)_e\right]\Delta\eta\ + \left[\left(-y_\xi P\right)_s - \left(-y_\xi P\right)_n\right]\Delta\xi \quad (3.37.a)$$

for x-momentum eqn, and

$$f(P) = \left[\left(-x_\eta P\right)_w - \left(-x_\eta P\right)_e\right]\Delta\eta + \left[\left(x_\xi P\right)_s - \left(x_\xi P\right)_n\right]\Delta\xi \quad (3.37.b)$$

for y-momentum eqn, and it is zero for other transport equations. Also the superscript 0 refers to the previous time level, and $\Delta\xi$, $\Delta\eta$, $\delta\xi_e$, $\delta\xi_w$, $\delta\eta_n$, and $\delta\eta_s$ are geometric lengths as shown in Figure 3.5; it is possible to take all of them as unity, which is one of the advantages of our method. The following explanations for the terms of the equation (3.36) are worthwhile.

3.6.1 Time Discretization

Solidification and melting are generally transient phenomena, where the explicit schemes are too restrictive owing to stability limitations. The implicit time schemes are generally not limited by the size of the time step and this trait is a good motivation for our selection. Hence, first order Euler scheme as a simplest implicit scheme were adopted in order to perform the required integration in time ,eqn (3.36) The first order scheme is a two-point scheme and take into account the value of function ϕ at the current and the previous time steps. More precise methods like

second-order implicit scheme, which is a three-point scheme for time integration, also can be used.

3.6.2 Discretization of convective Fluxes

Many different schemes have been proposed to discretize the convective term and among them the QUICK scheme has been found to offer solutions with high accuracy and at the same time have a good stability. Thus this discretization approach and the deferred-correction technique of Khosla and Rubin [25] is employed in the present study.

3.6.3 Diffusive Fluxes Treatment

The diffusive fluxes in the eqn (3.36) are split into two parts, orthogonal and nonorthogonal. In the eqn (3.36), first and second terms at the right hand side are orthogonal parts of diffusive fluxes, while third and fourth terms at the right hand side are nonorthogonal parts. The orthogonal part of the diffusive fluxes at face e, can be evaluated by using a central differential scheme in the computational space (direction ξ, see Figure3.5).

$$\Gamma\left(\sqrt{g}g^{11}\frac{\partial\phi}{\partial\xi}\right)_e \approx \Gamma\left(\sqrt{g}g^{11}\right)_e(\phi_E - \phi_P) \tag{3.38}$$

The orthogonal contribution along η coordinate is treated similarly. In order to restrict the size of the coefficient matrix of the algebraic system resulting from the discretization, the nonorthogonal part of the diffusive term, which is called the cross derivative term, is treated explicitly. The nonorthogonal portion for east face e, of a control volume can be written as

$$\Gamma\left(\sqrt{g}g^{12}\frac{\partial\phi}{\partial\eta}\right)_e \approx \Gamma\left(\sqrt{g}g^{12}\right)_e(\phi_{ne}-\phi_{se}) \tag{3.39}$$

The values of ϕ at the CV corner points (e.g., north east, ne) which do not lie in the computational seven-point stencil, need to be interpolated. For instance, a weighted linear interpolation can be used, i.e.,

$$(\phi_{ne}-\phi_{se}) \approx \frac{1}{4}(\phi_N+\phi_{NE}-\phi_S-\phi_{SW}) \tag{3.40}$$

where neighboring points of NE and SW are shown in Figure 3.6.

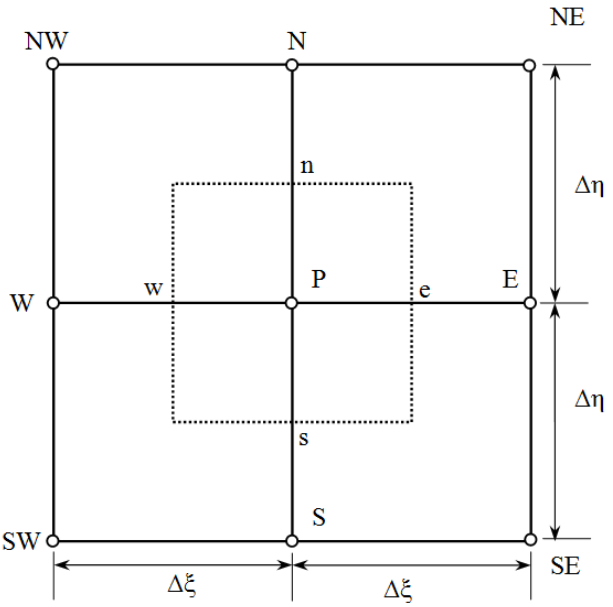

Figure 3.6: Neighboring points around the central node in computational plane.

3.6.4 Final form of discretized equations

By applying the abovementioned discretization methods to eqn (3.36), a general discretized equation, which links the value of dependent variable at the CV center with the neighboring values algebraically, can be acquired as

$$A_P\phi_P = \mathrm{A}_E\phi_E + \mathrm{A}_W\phi_W + \mathrm{A}_N\phi_N + \mathrm{A}_S\phi_S + \mathrm{A}_P{}^0\phi_P{}^0 + b_P + P_\phi \tag{3.41.a}$$

where

$$\mathrm{A}_E = \Gamma\left(\sqrt{g}g^{11}\right)_e + \max[-\mathrm{F}_e, 0] \tag{3.41.b}$$

$$A_W = \Gamma\left(\sqrt{g}g^{11}\right)_w + \max[-\mathrm{F}_w, 0] \tag{3.41.c}$$

$$A_N = \Gamma\left(\sqrt{g}\,g^{22}\right)_n + \max[-\mathrm{F}_n, 0] \tag{3.41.d}$$

$$\mathrm{A}_S = \Gamma\left(\sqrt{g}g^{22}\right)_s + \max[-\mathrm{F}_s, 0] \tag{3.41.e}$$

$$A_P = A_E + \mathrm{A}_W + A_N + A_S + A_P{}^0 - \sqrt{g}S_P \tag{3.41.f}$$

$$A_P{}^0 = \frac{\sqrt{g}^0}{\Delta t} \tag{3.41.g}$$

$$b_P = \mathrm{S}_\phi + b_1 + b_{cd} \tag{3.41.h}$$

$$\begin{aligned} b_1 = &-\max[F_e, 0]\,(\phi_e - \phi_P) + \max[-F_e, 0]\,(\phi_e - \phi_E) - \\ &\max[-F_w, 0]\,(\phi_w - \phi_P) + \max[F_w, 0]\,(\phi_w - \phi_W) - \\ &\max[F_n, 0]\,(\phi_n - \phi_P) + \max[-F_n, 0]\,(\phi_n - \phi_N) - \\ &\max[-F_s, 0]\,(\phi_s - \phi_P) + \max[F_s, 0]\,(\phi_s - \phi_S) \end{aligned} \tag{3.41.i}$$

$$F_e = (U)_e\ ,\ F_w = (U)_w\ ,\ F_n = (V)_n\ ,\ F_s = (V)_s \tag{3.41.j}$$

$$\begin{aligned} b_{cd} = &\left(\Gamma\sqrt{g}g^{12}\frac{\partial\phi}{\partial\eta}\right)_e - \left(\Gamma\sqrt{g}g^{12}\frac{\partial\phi}{\partial\eta}\right)_w + \left(\Gamma\sqrt{g}g^{21}\frac{\partial\phi}{\partial\xi}\right)_n \\ &- \left(\Gamma\sqrt{g}g^{21}\frac{\partial\phi}{\partial\xi}\right)_s \end{aligned} \tag{3.41.k}$$

where the term b_1 appears as a result of utilizing the deferred-correction procedure. By using eqn (3.40), the cross derivative term, b_{cd} , for the interior points, can be discretized as

$$
\begin{aligned}
b_{cd} = & \left(\Gamma \frac{g^{12}}{\sqrt{g}}\right)_e \left(\frac{1}{4}(\phi_N + \phi_{NE} - \phi_S - \phi_{SE})\right) \\
& - \left(\Gamma \frac{g^{12}}{\sqrt{g}}\right)_w \left(\frac{1}{4}(\phi_N + \phi_{NW} - \phi_S - \phi_{SW})\right) \\
& + \left(\Gamma \frac{g^{21}}{\sqrt{g}}\right)_n \left(\frac{1}{4}(\phi_E + \phi_{NE} - \phi_W - \phi_{NW})\right) \\
& - \left(\Gamma \frac{g^{21}}{\sqrt{g}}\right)_s \left(\frac{1}{4}(\phi_E + \phi_{SE} - \phi_W - \phi_{SW})\right)
\end{aligned} \tag{3.42}
$$

The values of Γ are defined in Table 2.1. S_ϕ is zero in all equations except y-momentum equation and it is given by $\sqrt{g} Ra \Pr \theta$. P_ϕ for each transport equation are zero except for x and y momentums and it is given by eqn (3.37).

From the discretized equations, it is clear that the velocities at the control volume faces (u_e, u_w, v_n, v_s) are needed in the continuity equation as well as the velocities at the cell-face center. However, in the collocated variable arrangement these values are not known at the cell-face centre. If the velocity of fluid at cell faces is carried out by a linear interpolation of velocity obtained by solving the momentum equations for collocated grids, nonphysical checkerboard velocity and pressure fields may appear, as explained by Patankar and Spalding [28]. Hence, an interpolation in an appropriate manner is required to express the cell-face values of the variables and their derivatives in terms of their nodal values. Rhie and Chow [27] proposed a remedy for this problem in which all other quantities are interpolated at cell faces except the velocity by the so-called momentum interpolation method. However, this method has shown to be dependent on underrelaxation factor as well as the time step size. To cope with this problem, we employed the reformed version of the so-called momentum interpolation method, proposed by B. Yu et al.[26], which is independent

of underrelaxation factor and the time step size. Here we only write down the results; as an example, the velocity of the right face of a control volume, u_e , can be interpolated as follows

$$u_e = \alpha_u \left(\frac{\sum_i A_i u_i + b_p}{A_p} \right)_e - \frac{\alpha_u \Delta y (P_E - P_P)}{(A_P)_e} + (1 - \alpha_u) u_e^0 \qquad (3.43)$$

where A_i is the coefficient of the neighboring points, α_u is the velocity correction factor and $b_p$is defined by eqn (3.41.h). The first term of the right hand side of the equation (3.43) can be interpolated as

$$\left(\frac{\sum_i A_i u_i + b_p}{A_p} \right) = \frac{(\sum_i A_i u_i + b_1)_E + (\sum_i A_i u_i + b_1)_P + \left[\left(S_\phi\right)_E + \left(S_\phi\right)_P \right]}{(\sum_i A_i)_E + (\sum_i A_i)_P - [(S_P)_E + (S_P)_P]} \qquad (3.44)$$

where b_1 is defined in eqn (3.41.i)and second and third terms in eqn (3.43) is interpolated as follows

$$(A_P)_e = \left(\sum_i A_i \right)_E + \left(\sum_i A_i \right)_P - [(S_P)_E + (S_P)_P] \qquad (3.45)$$

3.6.5 Space Conservation Law

Discretized form of the equation (3.30), whose time discretization method is the same as the time discretization method used for the discretization of the general conservation laws, is

$$\frac{\sqrt{g} - \sqrt{g}^0}{\Delta t} \Delta\xi \, \Delta\eta = \left[\left(U_g\right)_e - \left(U_g\right)_w \right] \Delta\eta + \left[\left(V_g\right)_n - \left(V_g\right)_s \right] \Delta\xi \qquad (3.46)$$

where superscript 0 stands for the last time level. As we mentioned previously, $\Delta\xi$ and $\Delta\eta$ are set to unity. Equation (3.46) relates the Jacobian and grid velocities at each cell.

There are two approaches for relating the Jacobian and the grid velocities. In the first approach grid and contravariant velocity vectors are calculated by estimating

the Jacobian (Demirdzic and Peric [18]) or the so called swept volume. In the second approach the value of the Jacobian is evaluated and updated by computing the grid and contravariant velocities and substituting them into equation (3.46) (Shyy et al [3]).

The last approach is adopted and for the sake of brevity only the last approach is discussed and we have not studied the first scheme here. Imagine a typical control volume moves by the time step, Δt. Contravariant grid velocities (U_g and V_g) can be determined on each face by eqn (3.31). To do so, we need to find u_g and v_g, the Cartesian grid velocities of the cell faces due to grid movement. These velocities can be calculated by a first order differentiation of displacement with time. As an example the Cartesian grid velocity of the east face along x direction, i.e. $(u_g)_e$, can be approximated at the east face by

$$(u_g)_e = \frac{\Delta x_e}{\Delta t} \tag{3.47}$$

where Δx_e is the displacement of the east face along x direction due to the grid movement. Similarly, we can approximate other cell face velocities and subsequently the contravariant grid velocities (U_g and V_g) at each face can be found by equation (3.31). Then the equation (3.46) can be utilized to find the Jacobian at the new time step, $\sqrt{g}$.

3.6.6 Pressure Velocity coupling

Solving the velocity field merely by means of momentum equations does not satisfy the continuity equation. Moreover, there is no explicit equation for the pressure term in the momentum equations, and the pressure is taken from the previous outer iteration. This coupling of velocity and pressure in the flow equations

is treated with the SIMPLE algorithm of Patankar and Spalding[28], in which a pressure-correction equation is solved to correct both pressure and velocity fields. The discretized continuity equation needs the velocity of fluid at cell faces and it is obtained by momentum interpolation method, discussed in section 3.6.4.

The pressure-correction equation is affected by the grid movement and can be written by

$$A_P P_P^{'} = A_E P_E^{'} + A_W P_W^{'} + \mathrm{A}_N P^{'}{}_N + A_S P^{'}{}_S + \frac{\sqrt{\mathrm{g}}^0 - \sqrt{\mathrm{g}}}{\Delta \mathrm{t}} + [(U^*)_w - (U^*)_e + (V^*)_s - (V^*)_n] \tag{3.48.a}$$

where the term P' stands for the corrected pressure and asterisk are the guessed values for fluxes. The coefficient of this equation can be written as

$$A_E = \left(y_\eta D_u^x - x_\eta D_v^x\right)_e \tag{3.48.b}$$

$$A_W = \left(y_\eta D_u^x - x_\eta D_v^x\right)_w \tag{3.48.c}$$

$$A_N = \left(-y_\xi D_u^y + x_\xi D_v^y\right)_n \tag{3.48.d}$$

$$A_S = \left(-y_\xi D_u^y + x_\xi D_v^y\right)_s \tag{3.48.e}$$

where the values of D_j^i can be determined by eqn (3.51). Having solved the pressure correction equation, the corrections in the contravariant and Cartesian velocities can be determined by

$$U_e^{'} = \left(y_\eta D_u^x - x_\eta D_v^x\right)_e (P_P^{'} - P_E^{'}) + \left(-y_\eta D_u^y - x_\eta D_v^y\right)_e (P_s^{'} - P_n^{'})_e \tag{3.49.a}$$

$$V_n^{'} = \left(x_\xi D_v^y - y_\xi D_u^y\right)_n (P_P^{'} - P_N^{'}) + \left(x_\xi D_v^x - y_\xi D_u^x\right)_n (P_w^{'} - P_e^{'})_n \tag{3.49.b}$$

$$u_P^{'} = (D_u^x)_P (P_w^{'} - P_e^{'})_P + \left(D_u^y\right)_P (P_s^{'} - P_n^{'})_P \tag{3.50.a}$$

$$v_P^{'} = \left(D_v^y\right)_P (P_s^{'} - P_n^{'})_P + (D_v^x)_P (P_w^{'} - P_e^{'})_P \tag{3.50.b}$$

where

$$D_u^x = \frac{\alpha_u y_\eta}{A_P^u} \tag{3.51.a}$$

$$D_u^y = -\frac{\alpha_u y_\xi}{A_P^u} \tag{3.51.b}$$

$$D_v^y = \frac{\alpha_v x_\xi}{A_P^v} \tag{3.51.c}$$

$$D_v^x = -\frac{\alpha_v x_\eta}{A_P^v} \tag{3.51.d}$$

Subsequently, the following equations are used to correct the guessed values such as velocities, pressure, and contravariant velocities in the SIMPLE algorithm.

$$U = U^* + U' \tag{3.52.a}$$

$$V = V^* + V' \tag{3.52.b}$$

$$(P)_P = (P^*)_P + \alpha_P (P')_P \tag{3.52.c}$$

$$(u)_P = (u^*)_P + (u')_P \tag{3.52.d}$$

$$(v)_P = (v^*)_P + (v')_P \tag{3.52.e}$$

3.6.7 Discretization of the Stefan Condition

Having the Stefan condition in the form of the equation (3.33), now we can discretize them by a straightforward finite difference method, and the result can be written as

$$\begin{aligned} u_{IN} &= 2\frac{ste}{\sqrt{g}^{IN}}\left(y_\eta\right)^{IN}\left\{\bar{k}[\theta_s^E - \theta_m] - [\theta_m - \theta_l^W]\right\} \\ v_{IN} &= -2\frac{ste}{\sqrt{g}^{IN}}\left(x_\eta\right)^{IN}\left\{\bar{k}[\theta_s^E - \theta_m] - [\theta_m - \theta_l^W]\right\} \end{aligned} \tag{3.53}$$

In the notation of the above equations θ_m refers to the interface temperature; the subscripts s and l, represent the solid and liquid state of the matter respectively,

and superscripts refers to the points in which the calculations are carried out; these points are illustrated in the Figure 3.7.

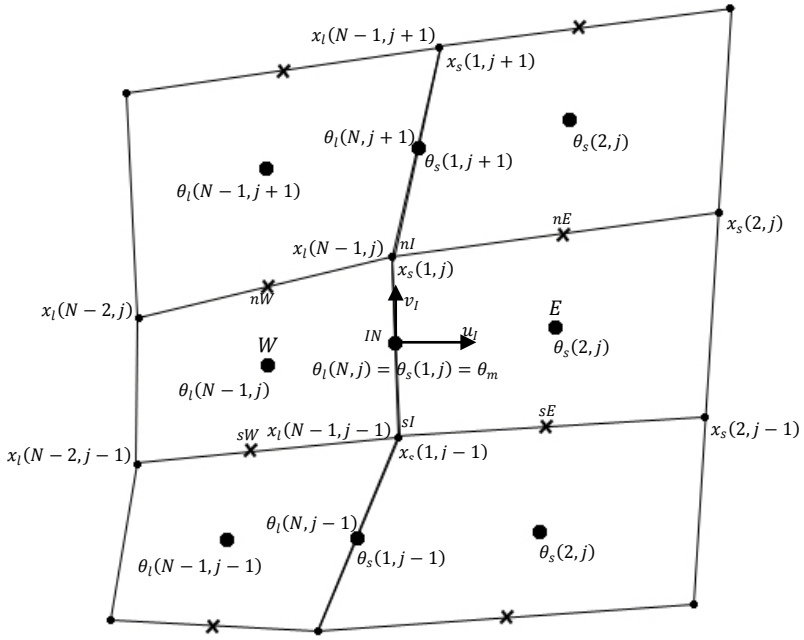

Figure 3.7: Interface and its contiguous control volumes. liquid region is at the left and solid is at the right of the interface.

After finding the computed interface velocity at the center of the control volume faces, the velocity of the vertices can be interpolated linearly, which in turn the new position of the grid can be computed.

3.7 Grid-Sliding Algorithm on the Interface

The moving-grid algorithm considered so far fairly can deal with simple phase-change problems. However, in the case of strong convection in the melt, the rate of heat transfer becomes nonuniform across the interface and hence the interface velocity varies from point to point. Subsequently, the numerical grids become clustered at regions with the lower rate of phase change and thus the quality of the

grids is worsened. It is therefore essential to devise an algorithm with which the numerical grid points on the interface can be redistributed. The physical location of the interface must maintain unchanged after the rearrangement of the nodes. In this work an algorithm based on cubic spline interpolation was employed. The new locations of the interface nodes were obtained in a manner that the distances between the adjacent nodes along the interface were taken to be equal. Figure 3.8 and 3.9 are depicted the arrangement of the grids before and after using grid-sliding algorithm on the interface.

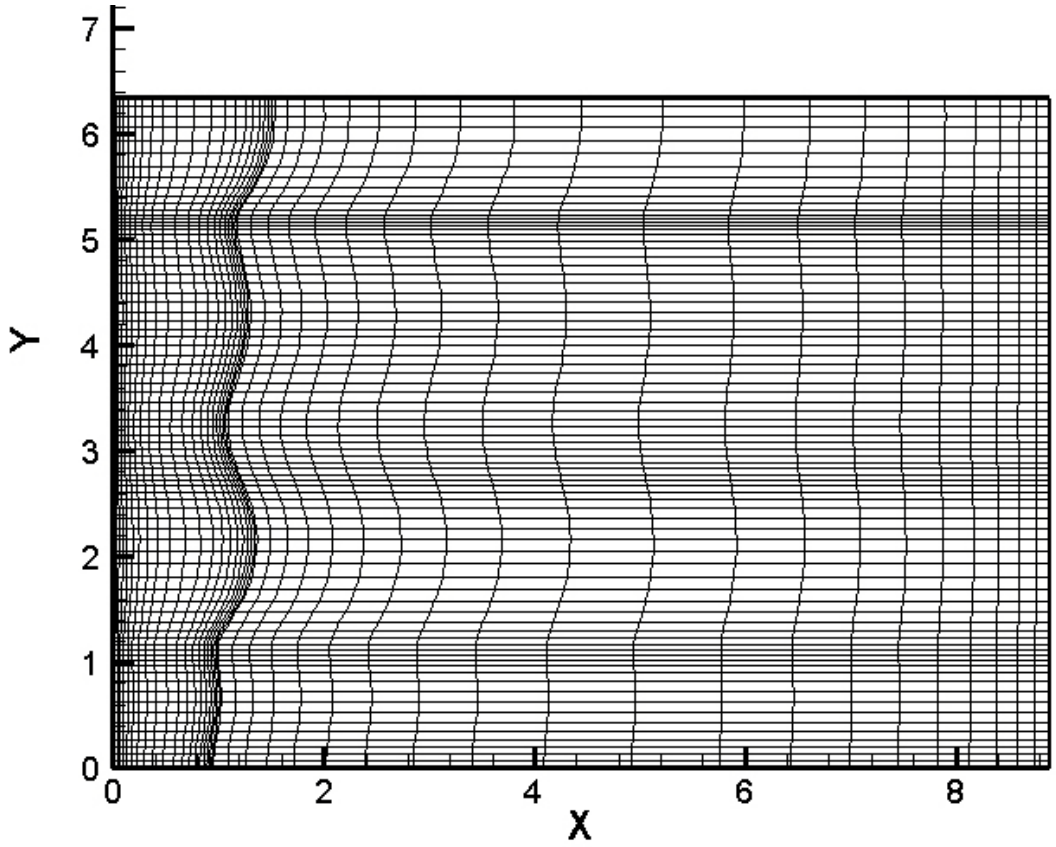

Figure 3.8: Grid distribution for gallium melting after $120s$ of process time without sliding algorithm.

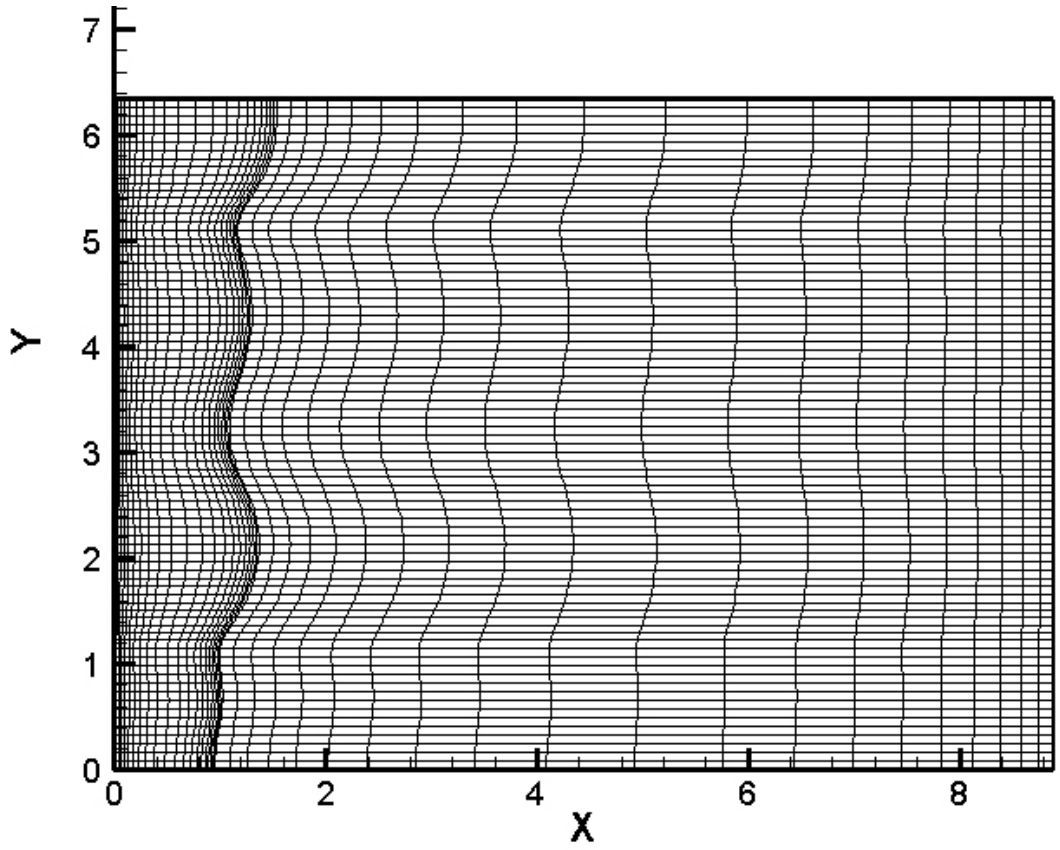

Figure 3.9: Grid distribution for gallium melting after $120s$ of process time with sliding algorithm.

3.8 Solution algorithm

The overall solution algorithm for the calculation of melting and solidification phenomena in irregular domains, by explicitly moving the phase-change interface, may now be summarized as follows, Figure 3.10.

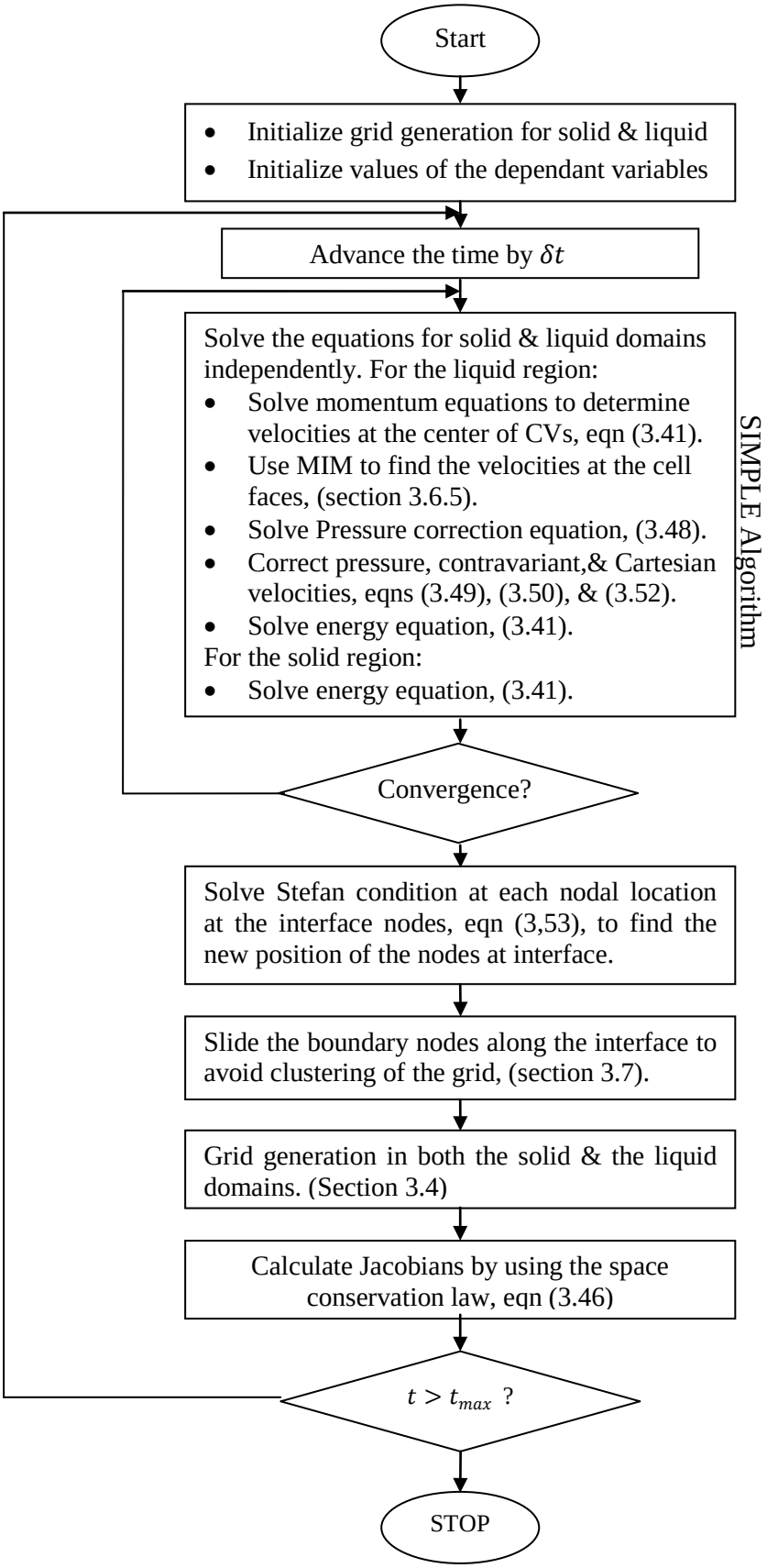

Figure 3.10: Solution Algorithm

CHAPTER 4

PROBLEM DESCRIPTION AND CODE VALIDATION

4.1 Introduction

To assess the strength of this numerical algorithm and verifying the code, a benchmark problem is chosen. The selection of this problem is because of the variety of available simulations which have performed by several researchers by using either a fixed grid or a transformed grid. Melting process has been investigated for pure Gallium; the exact calculation and the results are given in the following sections.

4.2 Melting in a rectangular cavity

The convection-dominated melting of pure gallium inside a cavity was simulated with the proposed algorithm as part of the validation exercise. The location of the interface after some time by taking advantage of the numerical calculations is compared with the results of Gau and Viskanta [24], in which the dimensional domain was consisted of a region $8.89\,cm$ long and $6.35\,cm$ high, which is shown by Figure 4.1. The top and bottom walls were assumed to be adiabatic, whereas the hot and cold side walls were considered to be isothermal. The cold wall was maintained at 28.3^0C. The temperature of the hot wall was suddenly raised to 38^0C, which initiated the melting process. To simulate this problem a very small liquid strip of 0.01% of the solid domain is considered at $t = 0$. The melting

temperature of gallium was taken as 29.78^0C. Table 4.1 illustrates the initial and boundary conditions and Table 4.2 presents thermophysical properties of liquid and solid gallium. As it can be seen, the upper and lower walls are subjected to adiabatic boundary condition. The left and right boundaries are imposed to hot and cold temperatures, respectively.

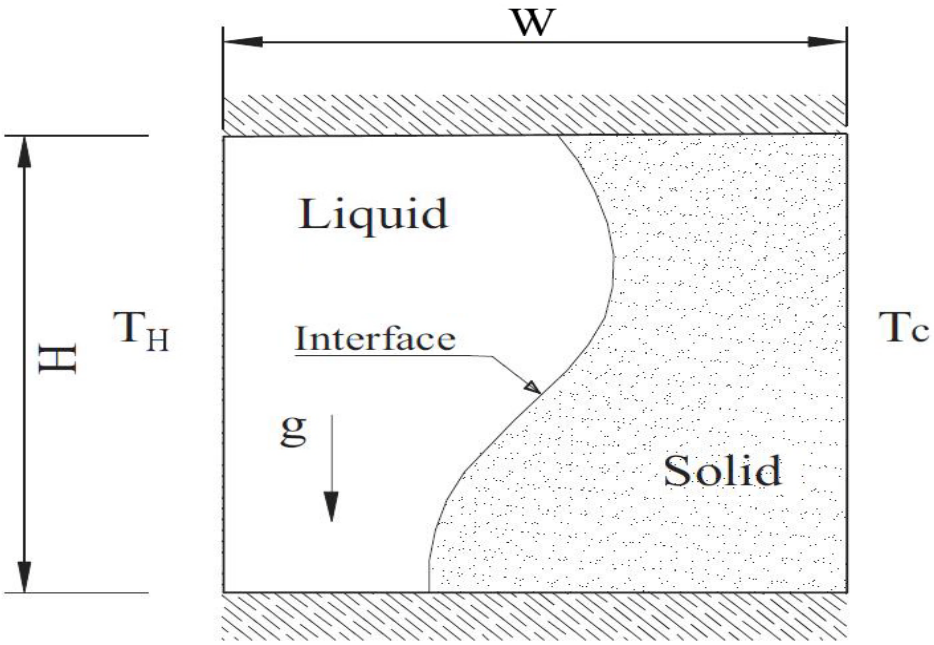

Figure 4.1: Schematic of the Problem.

Table 4.1: Boundary & Initial conditions in the gallium melting.

Boundary conditions	• $T_c = 28.3^0 C$ • $T_h = 38.0^0 C$ • $T_m = 29.78^0 C$ • No-slip condition at walls and solid-liquid interface. • Top and bottom walls are adiabatic. • Stefan condition at the interface
Initial conditions	• $T = 29.78^0 C$ • $x_{interface} = 0.01\ W$ • $u = v = 0$

Table 4.2: Thermophysical properties of liquid and solid gallium.

	Property	Value	Unit
Gallium (liquid)	k	32.0	$W\ /m\ K$
	c_{pl}	381.5	$J\ /kg\ K$
	ρ	6093	kg/m^3
	h_{sf}	8.016×10^4	$J\ /kg$
	μ	1.81×10^{-3}	$N\ s\ /m$
	β_T	1.20×10^{-4}	$1\ /K$
Gallium (solid)	k_s	32.0	$W\ /m\ K$
	c_{ps}	381.5	$J\ /kg\ K$
	ρ	6093	kg/m^3
	T_m	29.78	℃

Non-dimensional parameters can be obtained as follows:

$$\nu = \frac{\mu}{\rho} = 2.97 \times 10^{-7}\ m^2/s$$

$$\alpha_l = \frac{k}{\rho c_P} = 1.38 \times 10^{-5}\,\frac{m^2}{s}$$

$$Pr = \frac{\nu}{\alpha} = 0.0216$$

$$L_{ref} = 0.0635\ m\ , \quad x = \frac{x^*}{L_{ref}} = 1.4\ , \quad y = \frac{y^*}{L_{ref}} = 1$$

$$u_{ref} = \frac{\alpha_l}{L_{ref}} = 2.17 \times 10^{-4}\ m/s$$

$$\theta = \frac{T - T_c}{T_h - T_c}\ , \ \theta_h = 1\ , \quad \theta_c = 0\ , \quad \theta_m = 0.153$$

$$\theta_{initial} = 0$$

$$\Delta T = T_h - T_c = 9.7\ K\ , \quad Ste = \frac{C_p \Delta T}{h_{sf}} = 0.046$$

$$Ra = \frac{g\beta\Delta T L_{ref}^3}{\nu\alpha} = 7.0 \times 10^5$$

$$t^* = 0.1sec, \qquad t = \frac{t^*}{L_{ref}/u_{ref}} = 3.416 \times 10^{-4}$$

4.3 Benchmark Results

The problem was simulated until 600 *s* of process time with the time step of 0.1 seconds. Both solid and liquid domains are divided into 30×80 numbers of control volumes. Figure 4.2 shows a comparison of the interface locations obtained from present computations with the experimental results of Gau and Viskanta [24], as well as the numerical results of Jana et all. [9] at two different times.

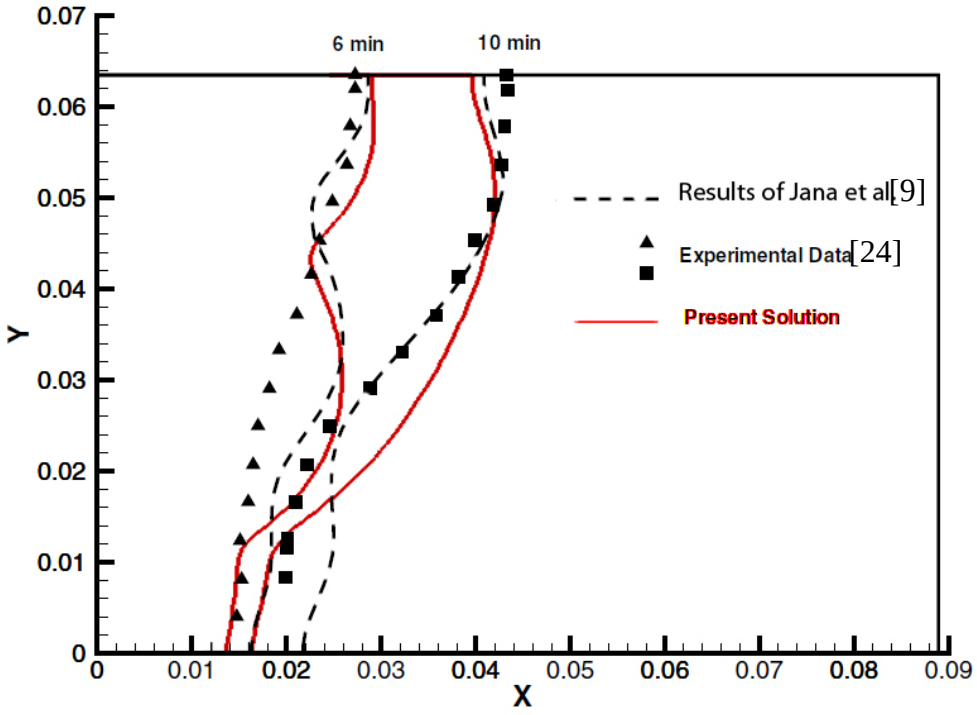

Figure 4.2: Gallium melting: validation of interface positions at 6 and 10 min with experimental results of Gau and Viskanta[24] and numerical results of Jana et al.[9].

In Figure 4.3 the interface configuration and streamlines are illustrated for five different time steps. The shape of the interface and number of the rolls of the streamlines shows conformity with the results of the Jana et al.[9], Figure 4.4.

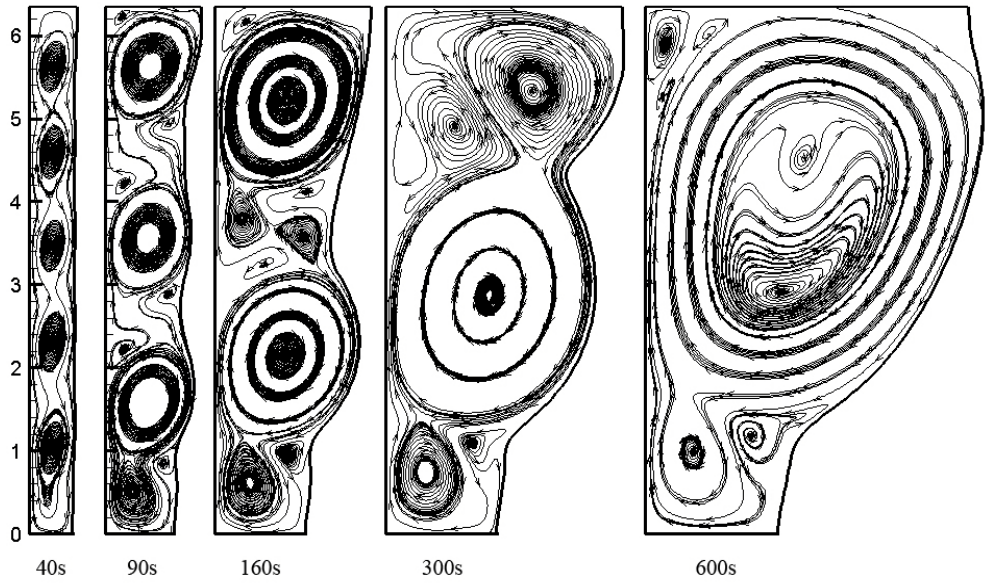

Figure 4.3: Gallium melting, streamlines and interface at several times during the melting process. Grid 30×80

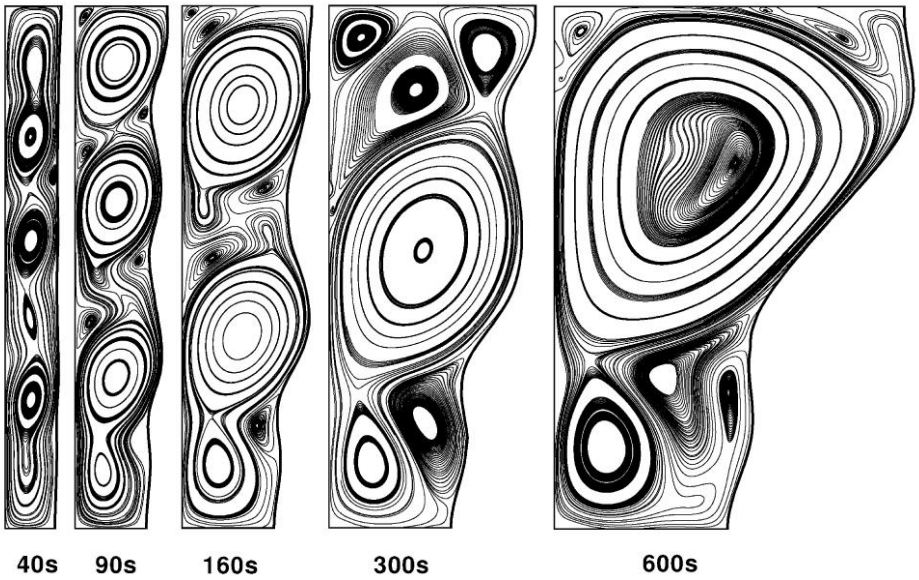

Figure 4.4: Gallium melting, the results of Jana et al [9]. Grid 30×80

CHAPTER 5

RESULTS AND DISCUSSIONS

5.1 Introduction

As it is illustrated in Figure 4.3, at early times, the solid-liquid interface is almost straight, indicating that conduction heat transfer is predominant. By the progression of time buoyancy driven natural convection in the liquid gallium start influencing the local heat transfer rate at the solid-liquid interface, which leads to distortion of the interface into curvature. At early times and with a weak advection heat transfer, the temperature of the fluid adjacent to the hot wall increases, results in the rise of the fluid. The liquid Gallium reaches to the top of the melt layer. Subsequently, the flow is deflected and descends along the interface and its temperature cooled down to nearly its fusion temperature. However, after a few seconds the flow is altered into multicellular structure. At nearly $t = 40s$, when the multicellular structure is well established, five flow cells are observed. These rolls are weak in strength and they are not able to cause deformation in the interface. Gradually, these rolls merge with each other and give rise to three major rolls of relatively higher strength. These vortices boost the heat transfer to the Solid-liquid interface. Accordingly, the melting rate increases locally at the position where the rolls are present and it brings about a few bulges at the interface, (See fig 4.3 at $160s$).

5.2 Resolving a Controversy

The present predictions show that the shape of the interface has separate bulges. This can be attributed to the multicellular structure of the flow in two-dimensional analysis, (Figure 4.3). The multicellular structure in the flow of the melted gallium was reported by many researchers and it was a controversial issue between former researchers. Earlier studies of fixed-grid methods failed to provide a correct flow features and this discrepancy occurred due to lack of sufficient grid resolution. However, employing very-large-resolution grids (up to 1120×800) by latter researchers like Hannuon et al[29] confirmed the multiple cellular features in gallium melting.

Moving grid methods are able to capture the flow features of Gallium melting even on coarse-grid simulations and it was firstly reported by Dantzig[30]. The present moving-grid method is also able to detect the rolls in the melt. The next section is discusses more about this issue.

5.3 Time step variation

Owing to the fact that in the gallium melting simulation Rayleigh number is relatively substantial, selecting the time steps larger than 0.1 seconds is not problem free. In other words, in order for the solution not to diverge, the increment of the Rayleigh number implies the reduction of the time step. However, the variation of the time step, as is illustrated in the Figure 5.1, only slightly affects the results.

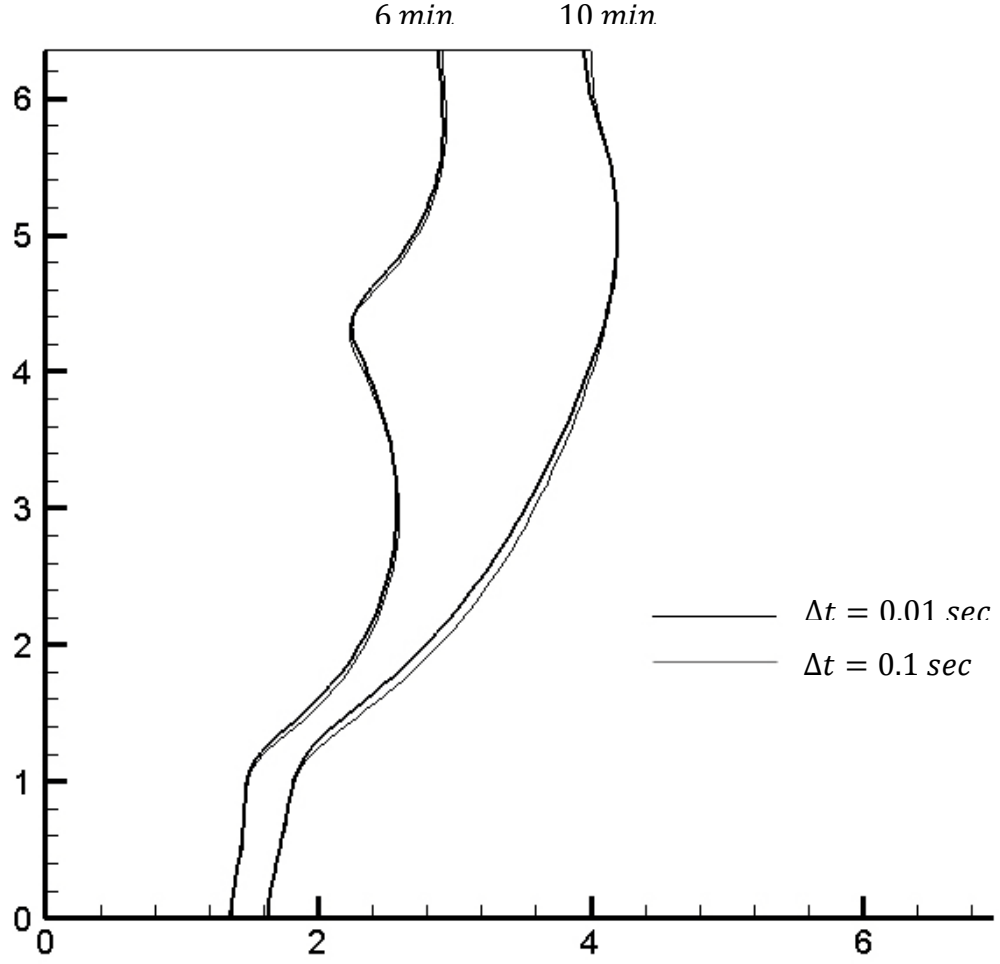

Figure 5.1: Interface position after 6 and 10 min using different time steps

5.4 Grid Refinement Test

We compare the flow structure and interface position for seven different numbers of grids and results are presented at five different times [Figure 5.2-5.8Figure 5.8]. The Rayleigh and Stefan numbers as well as the time step are same with the benchmark problem, i.e. $Ra = 7 \times 10^5$, $Ste = 0.046$, and $\Delta t = 0.1$.

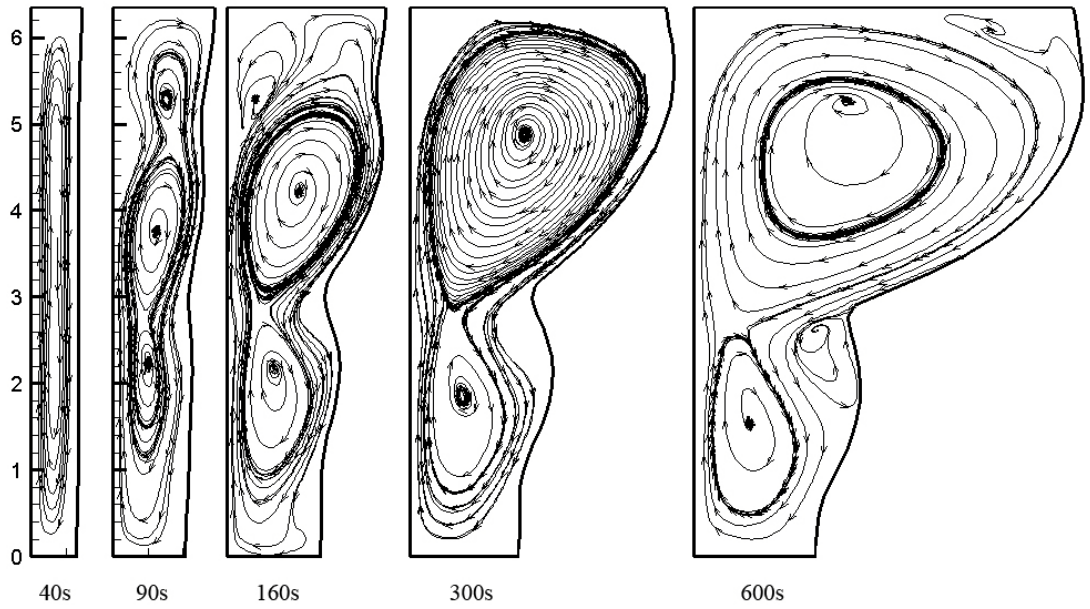

Figure 5.2: Streamlines and interface at several times during the melting process, : 10×40 grids.

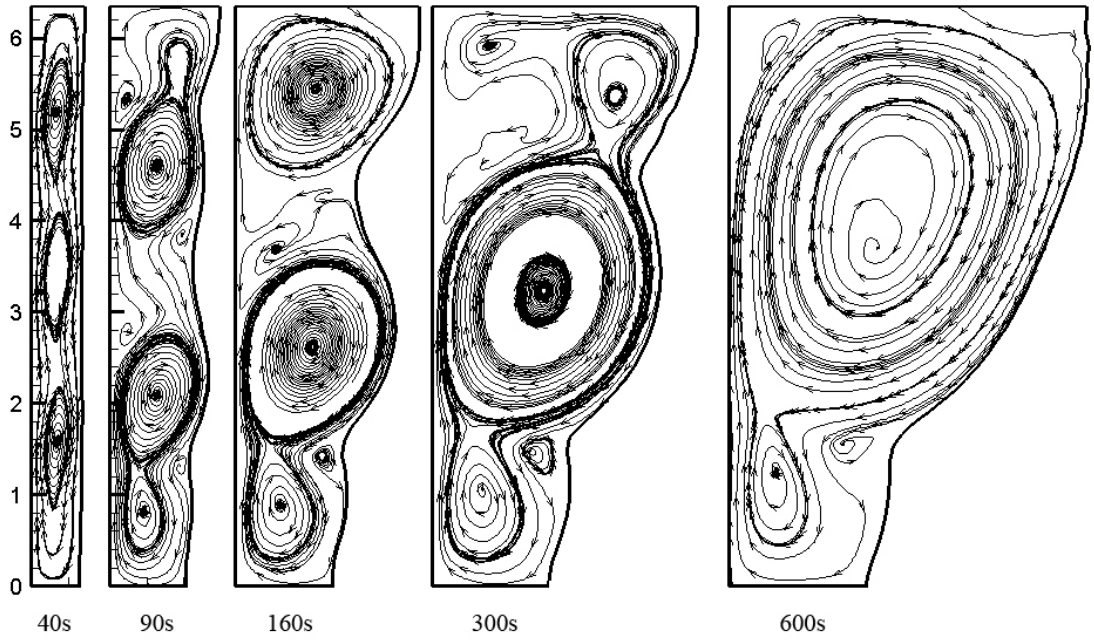

Figure 5.3: Streamlines and interface at several times during the melting process, 20×40 grids

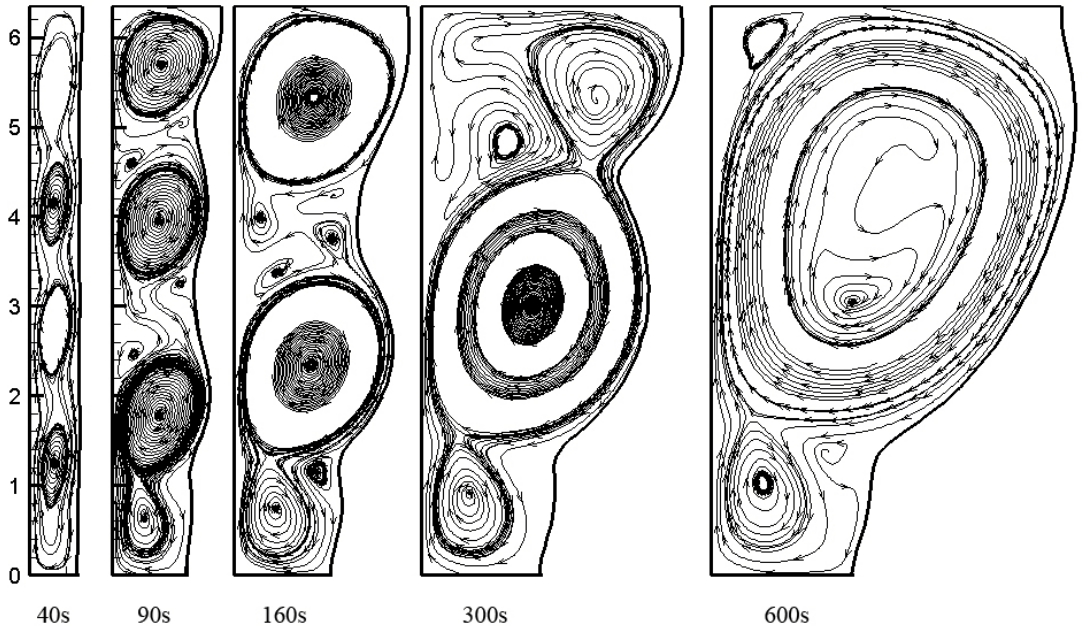

Figure 5.4: Streamlines and interface at several times during the melting process, 20×60 grids

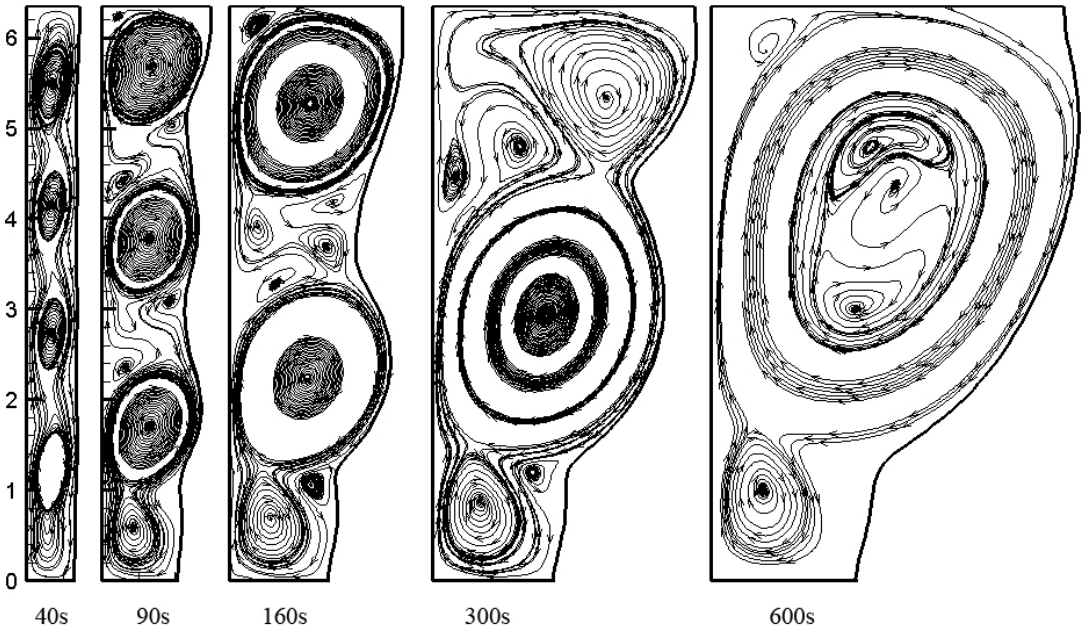

Figure 5.5: Streamlines and interface at several times during the melting process, 20×80 grids.

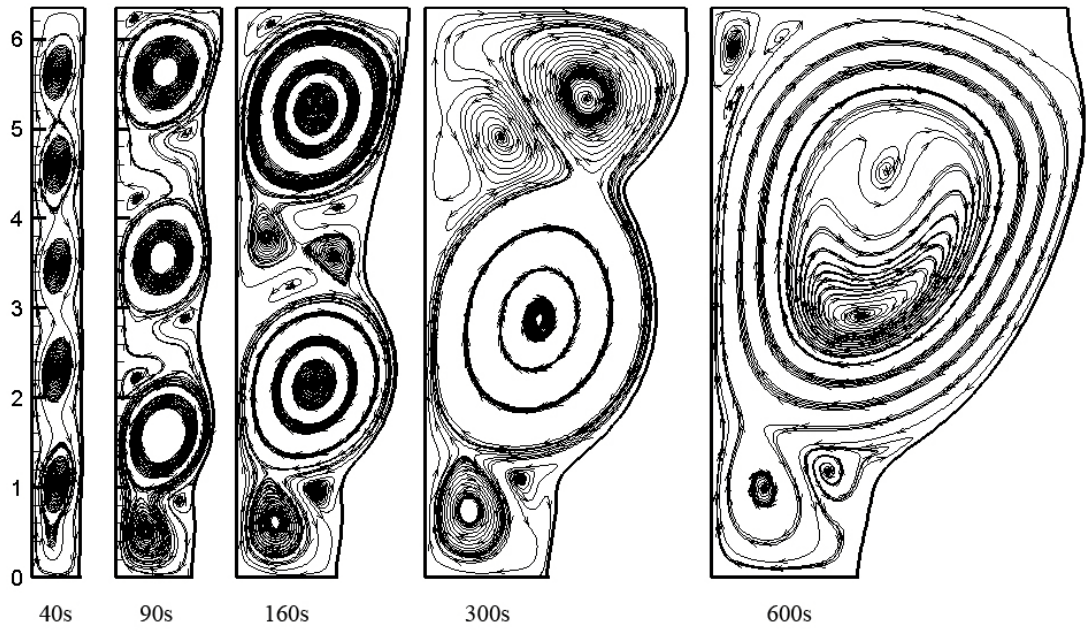

Figure 5.6: Streamlines and interface at several times during the melting process, 30×80 grids.

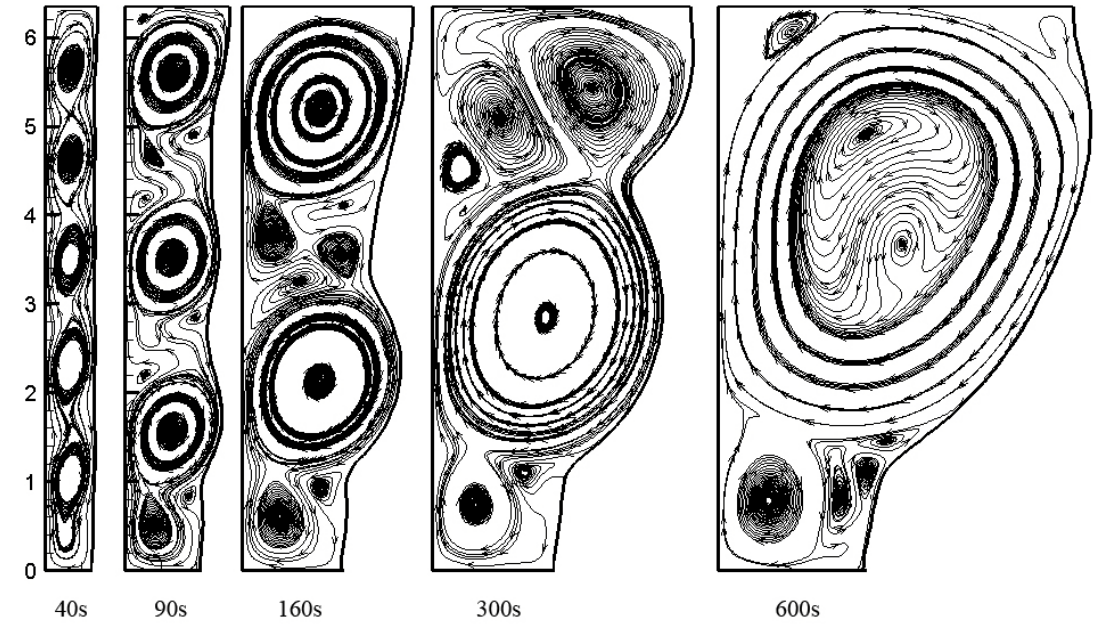

Figure 5.7: Streamlines and interface at several times during the melting process, 40×80 grids.

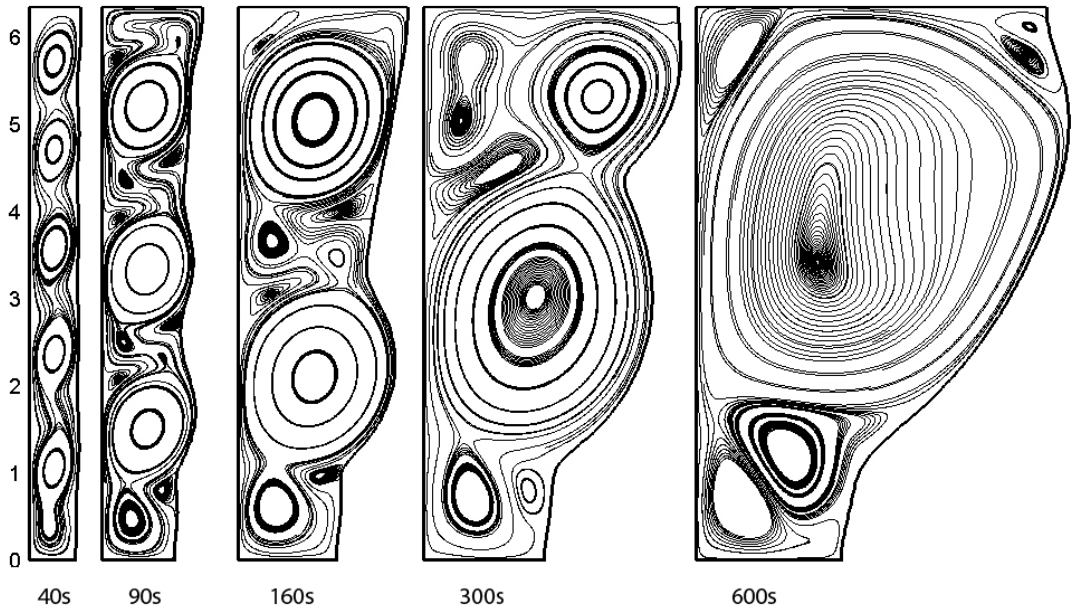

Figure 5.8: Streamlines and interface at several times during the melting process, 60×160 grids.

As it is evident, the number of rolls and the interface location is ascribed to the number of grids. Table 5.1 summaries the number of flow cells at $t = 40s$, when the rolls are well established. The higher the resolution of the grids, the higher of the number of rolls in the molten liquid, and the more precise is the solution. This trend continues up to nearly 30×80 control volumes in the melt above which the number of rolls become independent of the number of grids. Therefore the rest of the simulations are conducted with 30×80 CVs at each region.

The shape of the interface also depends on the number of grids (Figure 5.9). The 10×40 grids is failed to track the interface appropriately. As the number of grids increases the interface profile approximately approaches to a unique configuration.

Table 5.1: Number of flow cells for different number of grids at $t = 40s$.

Number of CVs in the melt	Number of Rolls
10×40	1
20×40	3
20×60	4
20×80	4
30×80	5
40×80	5
60×160	5

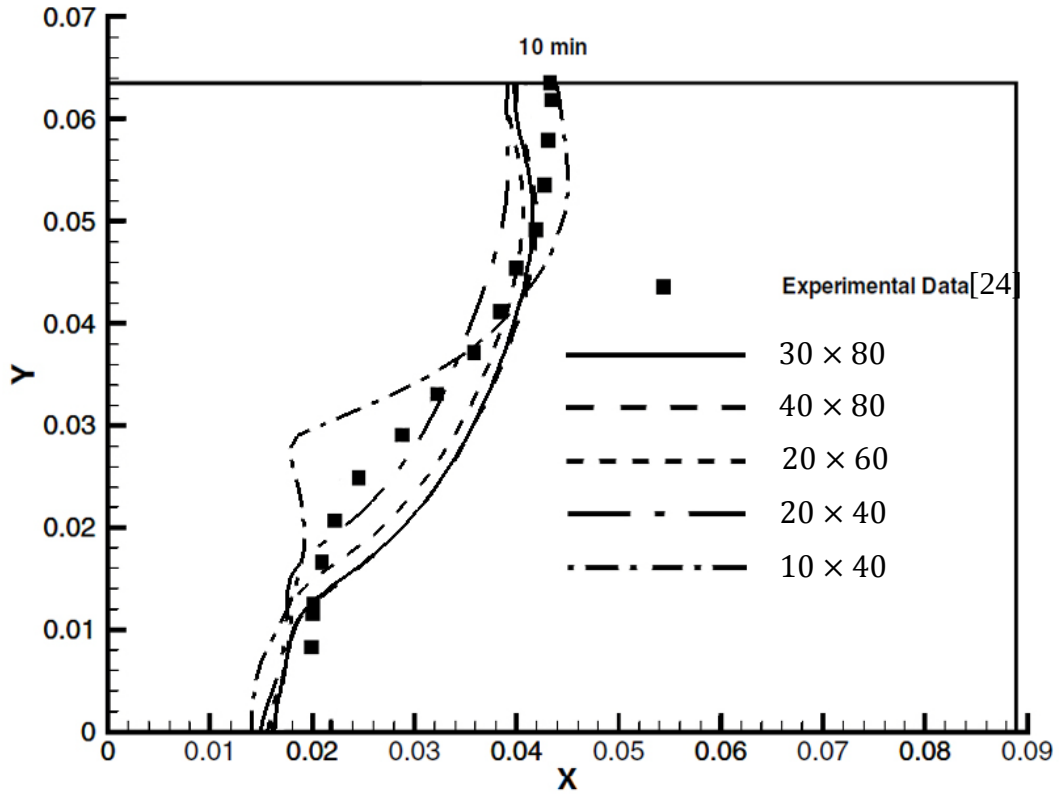

Figure 5.9: Solid-liquid interface for several grid sizes at $t = 10\ min$.

Now it is worth mentioning that not only the grid resolution plays an important role in the results, but also the configuration of the grids is crucial for the outcome. In Figure 5.10 the interface location is presented with two different grid distributions, namely, by adopting a grid generation using differential equation with equal spacing on the boundaries, as well as, utilizing the algebraic grid generation with dense grids near the walls. At the time $t = 190s$, a few seconds before the divergence of the computation in the domain with differential grid generation, interface location was compared between the two approaches. It is evident that the abovementioned differential grid generation distorted severely from the correct results. This situation even becomes worse when the number of grids is increased.

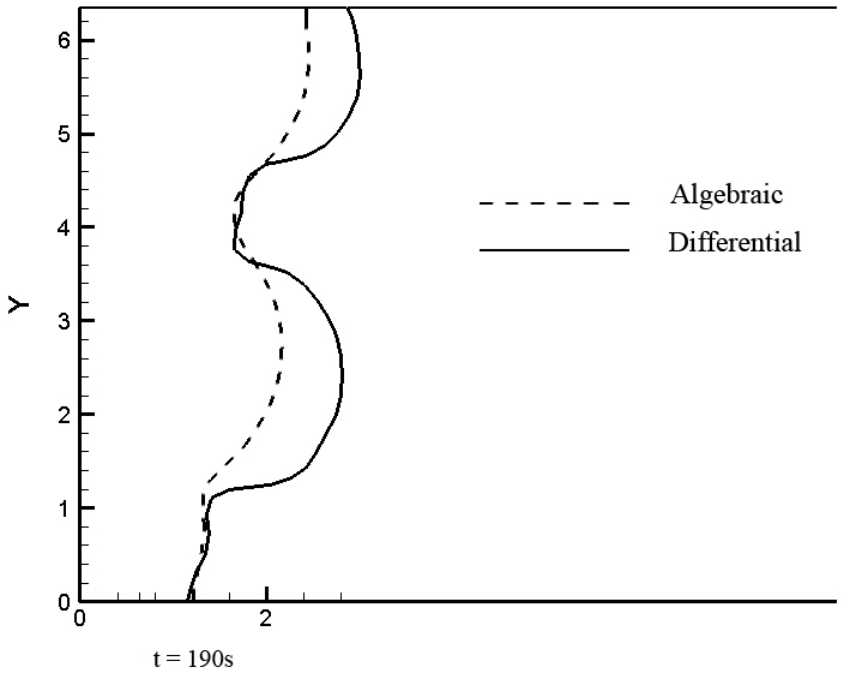

Figure 5.10: 20×80 Algebraic grid generation with the dense grid spacing near the wall vs. 20×80 differential grid generation with equal spacing on boundaries

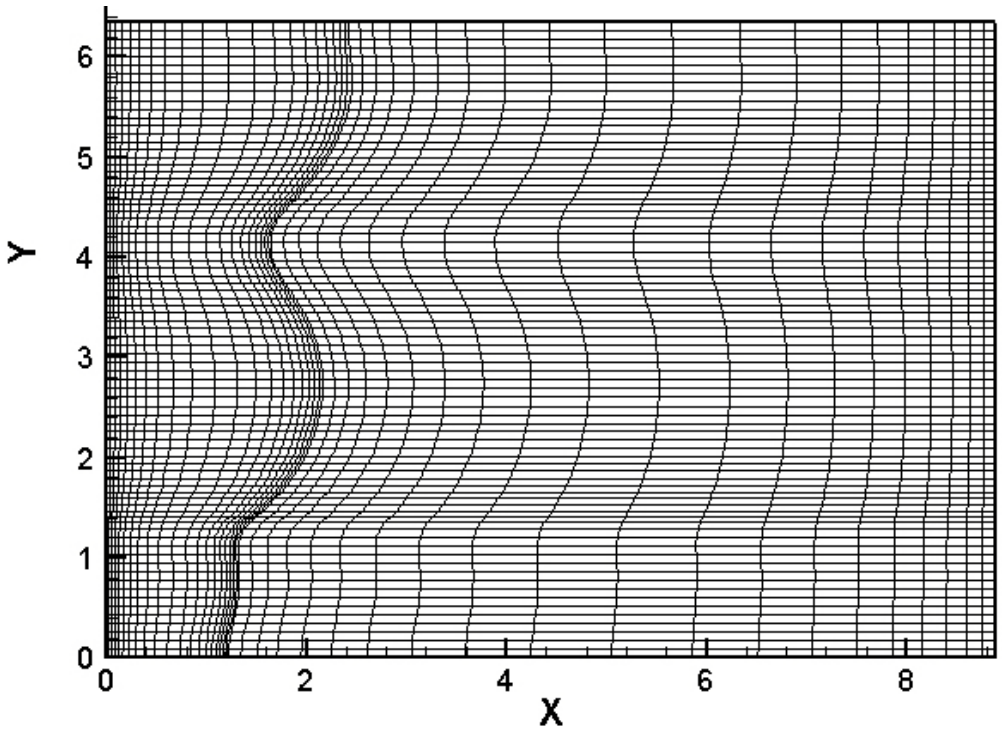

Figure 5.11: Grid generation using algebraic eqn. 20×80 grids at each region.

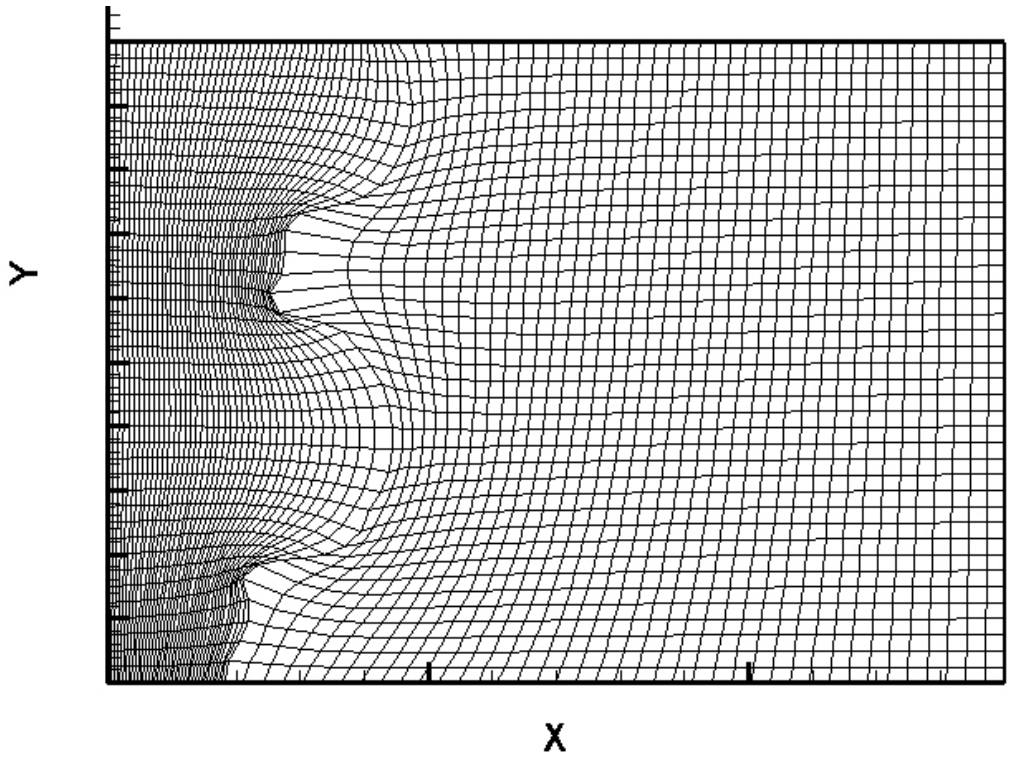

Figure 5.12: Grid configuration of the present differential grid generation with equal spacing on the boundaries, before divergence. 20×80 grids at each region.

5.5 Effect of Rayleigh Number

The Rayleigh number is a dimensionless number and its amount manifests the supremacy of convection or conduction inside the buoyancy driven flow of liquid. The high Rayleigh number is the representation of the strength of convection within a fluid body, while the low Rayleigh number implies that the conduction surmount the convection mode of heat transfer. Having set all of the variables to constant, in the following figures the influence of four different Rayleigh number on the flow structure as well as the interface shape are illustrated at various times, (Figure 5.13-Figure 5.17).

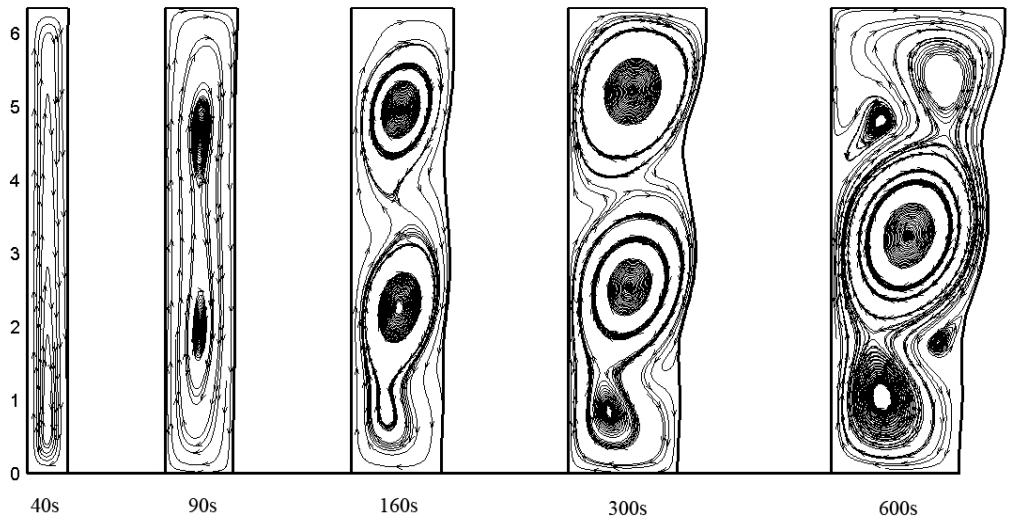

Figure 5.13: Streamlines and interface at several times during the melting process, $Ra = 7.0 \times 10^4$.

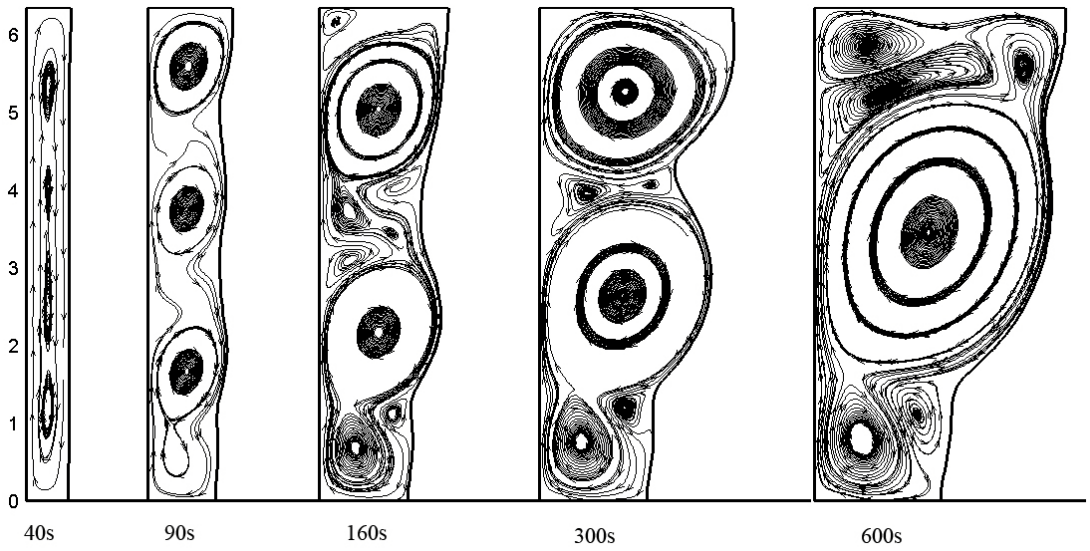

Figure 5.14: Streamlines and interface at several times during the melting process, $Ra = 3.5 \times 10^5$

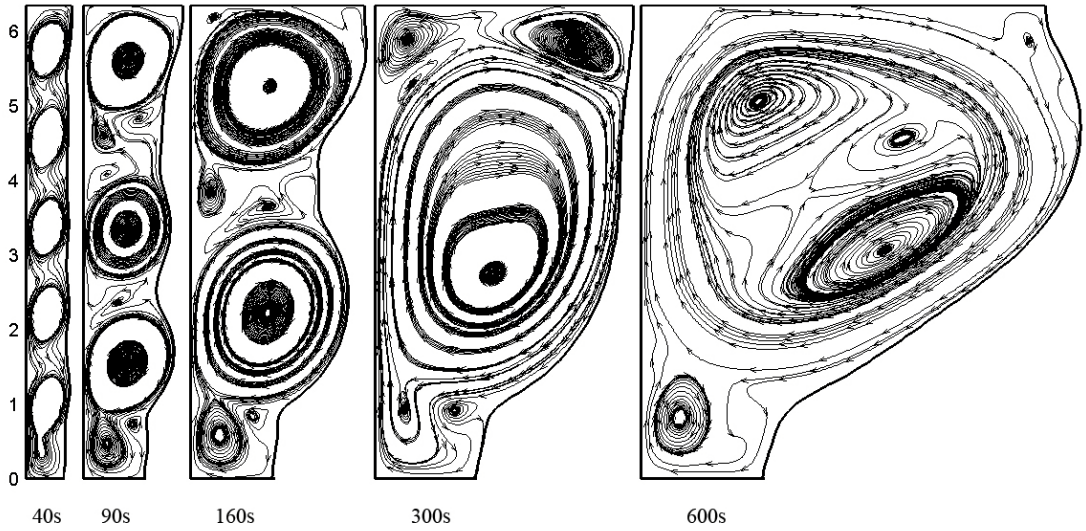

Figure 5.15: Streamlines and interface at several times during the melting process, $Ra = 1.4 \times 10^6$

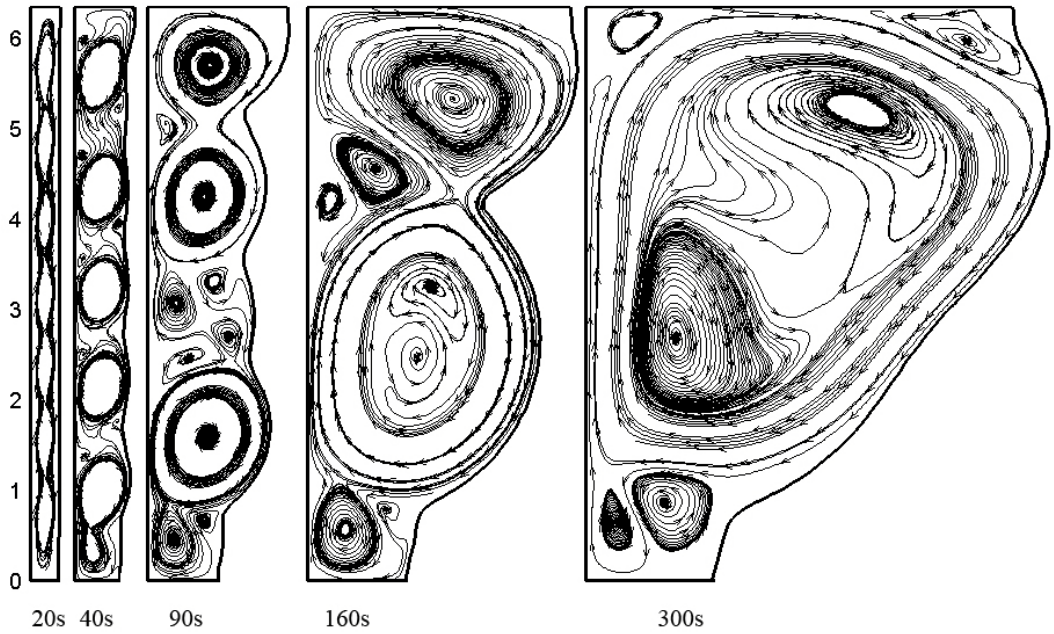

Figure 5.16: Streamlines and interface at several times during the melting process, $Ra = 2.8 \times 10^6$

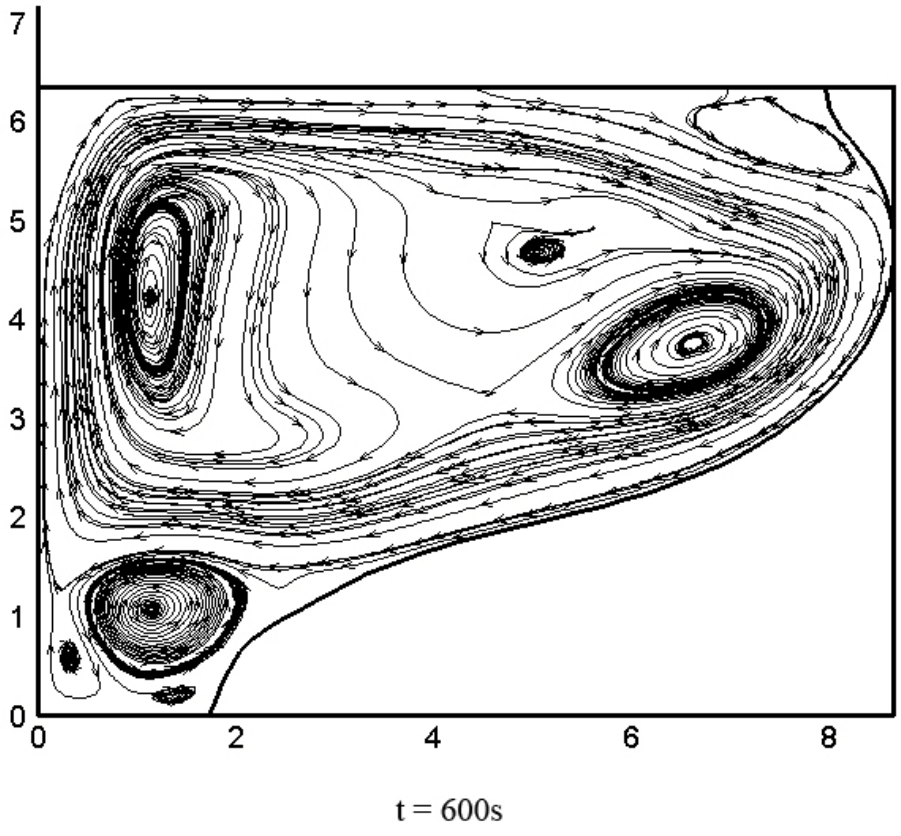

Figure 5.17: Streamlines and interface at $600s$ during the melting process, $Ra = 2.8 \times 10^6$

As we expected increment of Rayleigh number expedites the melting process and on the contrary its reduction reduces the effects of convection heat transfer and number of rolls. In Figure 5.16 the inauguration of seven rolls of vortices at $t = 20s$, implies the strength of the convective mode of heat transfer at early stages of melting. These rolls are merged together and create a powerful convection in a way that coincidently at $600s$ the interface reaches to the end of the cavity and stops the calculations.

5.6 Effect of Stefan Number

Stefan number is described as the ratio of sensible heat to latent heat. The higher of the Stefan number, the more amount of sensible heat compared to latent heat, and the fastest growth of melting or solidification. To study the influence of the Stefan number on the interface position and flow structure we maintains all of the variables as constant and we change the Stefan number. This test carried out for two different Stefan numbers, namely, $Ste = 0.23$ and $Ste = 0.01$. The following figures depict the effect of changing the Stefan number.

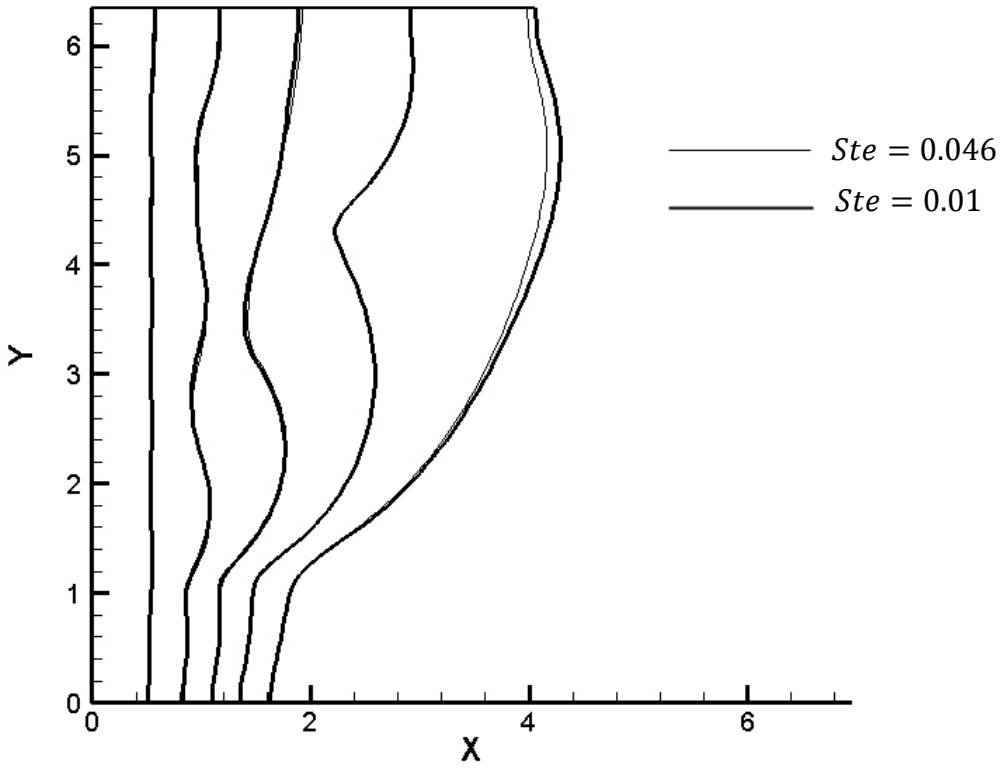

Figure 5.18: The corresponding time level from left to right.
For $\Delta t = 0.046$, $t = 40, 90, 160, 300, 600$s respectively.
For $\Delta t = 0.01$, $t = 180, 410, 740, 1380, 2760s$ respectively.

It seems that by reducing the Stefan number the interface evolution velocity reduced linearly until the fourth time level and at the fifth time level its differences arise itself, Figure 5.18.

In the next example the streamlines for the $Ste = 0.23$ is discussed

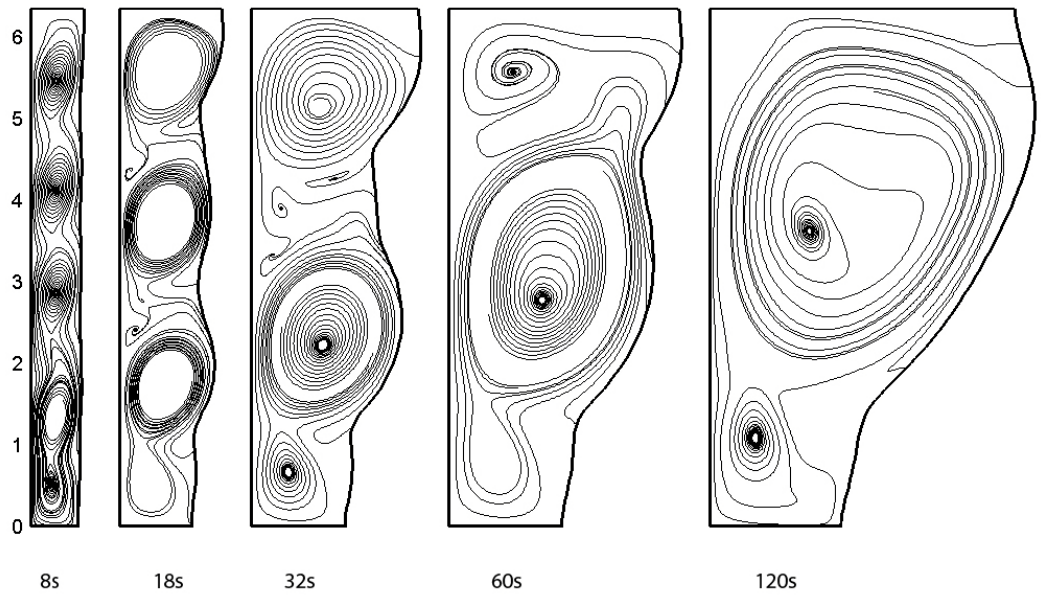

Figure 5.19: Streamlines and interface at different times during the melting process, $Ste = 0.23$.

In Figure 5.19, we increase the Stefan number five times greater than the original model. At $t = 8s$ the flow structure is established and the number of rolls is lower than the original model. This occurrence can be accounted for by the rate of the melting, which hinders the full formation of the rolls.

5.7 Change in physical volume

The Jacobian of the transformation expresses the volume of CVs in the physical coordinates. Using equation (3.15), we can determine the approximate physical volume. Physically, this volume must be constant, and as it is observed from Figure 5.20, the accumulation and disappearance of physical volume during the whole simulation is inconsistent with the reality. However, this inconsistency seems to be ineffectual in the final results and it is not felt by the numerical algorithm. The employment of the space conservation law by the method of Shyy et al [3], which is

stated in the section 3.6.5, is responsible for occurring this issue, and it was mentioned previously by Kumar et al[10].

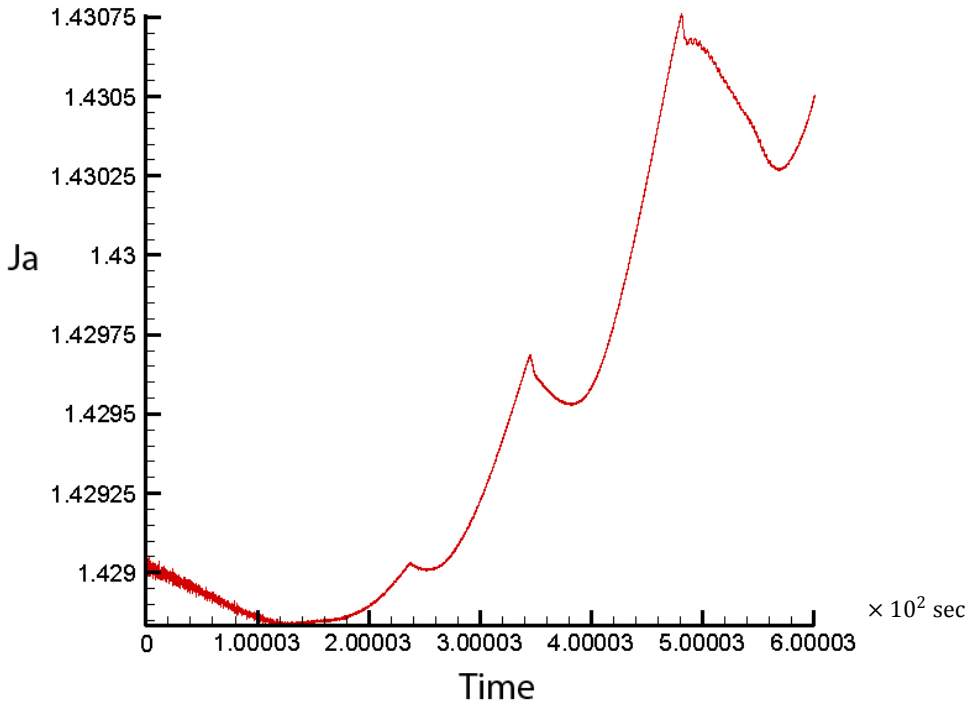

Figure 5.20: Summation of the Jacobian in the whole domain

CHAPTER 6

CONCLUSIONS

Understanding melting and solidification processes is of utmost importance in many fields of engineering. In this work a numerical study of melting of pure gallium at the vertical wall is performed. Two different domains for solid and liquid media are considered and the corresponding conservation equations on generalized curvilinear coordinates is solved, with a collocated variable arrangement.

The flow structure and interface position have been studied under different Rayleigh and Stefan numbers to deduce the importance of natural convection on the melting process.

It is understood that the grid generation play a crucial role on the results. Field values should be accurate near the boundaries and especially adjacent to the interface. Otherwise, it was noted that the interface configuration deviates severely. Thus, contraction of the grids near the interface is necessary and to do so we generated grids using algebraic methods in which near the interface and vertical walls have more dense grids. The present work shows that this grid generation can easily be carried out and an efficient method has been developed to adapt the grid after each time step to the new interface location, by taking the space conservation law into account.

In order to prevent clustering of the nodes on the interface arising due to buoyancy-induced convective flow in the melt and in the regions with high melting rates, a Cubic-Spline algorithm was employed to redistribute the grid points on the interface. If no grid smoothing was employed, the grid skewness led to divergence at early stages of the computations.

The Stefan condition was transformed by the nonconservative form of the gradient operator, and the conservative form of the equation was failed to present accurate results.

Virtually, melting and solidification processes have the characteristic of three dimensions. The present two-dimensional analysis neglects the influence of the third dimension and therefore has some drawbacks. For instance, the present predictions show that the shape of the interface has separate bulges which were otherwise nonexistent in the experimental observations and it is caused due to the absence of third dimension in the simulation [10]. The results obtained are encouraging and suggest the extension of the present method to three dimensional phase change analysis.

REFERENCES

[1] V. Alexiades, A. D. Solomon, Mathematical Modeling of Melting and Freezing Processes, Taylor and Francis, London, 1993.

[2] V.R. Voller, M. Cross, P.G. Walton, Assessment of weak solutions for solving Stefan problems, in: R.W. Lewis, K. Morgan (Eds.), Numerical Methods in Thermal Problems, Pineridge Press, Swansea, 1979, pp. 172–181.

[3] W. Shyy, H.S. Udaykumar, M.M. Rao, R.W. Smith, Computational Fluid Dynamics with Moving Boundaries, Taylor and Francis, London, 1996.

[4] V.R. Voller, M. Cross, N.C. Markatos, An enthalpy method for convection diffusion phase change, Int. J. Numer. Methods Eng. 24 (1987) 271–284.

[5] M. Zerroukat, C. R. Chatwin, Computaional Moving Boundary Problems, Research Studies Press Ltd., 1994.

[6] J. D. Anderson, Jr., Computational Fluid Dynamics, McGraw-Hill, 1995.

[7] A.W. Date, Novel enthalpy formulation for multidimensional solidification and melting of a pure substance, Sadhana 19 (1994) 833– 850.

[8] A.D. Brent, V.R. Voller, K.J. Reid, Enthalpy-porosity technique for modelling convection diffusion phase change: application to the melting of a pure metal, Numer. Heat Transfer 13 (1988) 297–318.

[9] S. Jana, S. Ray, and F. Durst, A numerical method to compute solidification and melting processes, Applied Mathematical Modeling, 31 (2007) 93-119

[10] V. Kumar, F. Durst, and S. Ray, Modeling moving-boundary problems of solidification and melting adopting an arbitrary Lagrangian-Eulearian approach, Numer. Heat Transfer, Part B, 49; 299-331, (2006)

[11] T. R. Goodman, the Heat-Balance Integral and Its Application to Problems Involving a Change of Phase, Trans. ASME 80, 335-342 (1958).

[12] H. S. Carslaw, J. C. Jaeger (eds.), Conduction of heat in solids, Clarendon Press, Oxford (1959).

[13] C.W. Hirt, B.D. Nichols, Volume of Fluid (VOF) methods for the dynamics of free boundaries, J. Comput. Phys. 39 (1981) 201-225.

[14] J. H. Ferziger, M. Peric, Computational Methods for Fluid Dynamics, Springer-Verlag, Berlin Heidlberg, 1996.

[15] S.W.J. Welch, J. Wilson, A volume of fluid based method for fluid flows with phase change, J. Comput. Phys. 160 (2000) 662–682.

[16] M. Sussman, P. Smereka, S.J. Osher, A level set approach for computing solutions to incompressible two-phase flow, J. Comput. Phys. 114 (1994) 146–159.

[17] A.A. Wheeler, W.J. Boettinger, G.B. McFadden, Phase field model for isothermal phase transitions in binary alloys, Phys. Rev. A 45 (1992) 7424.

[18] I.Demirdzic´, M. Peric´, Finite volume method for prediction of fluid flow in arbitrary shaped domains with moving boundaries, Int. J. Numer. Methods Fluids 10 (1990) 771–790.

[19] M. Farrashkhalvat and J.P. Miles, Basic Structured Grid Generation with an Introduction to Unstructured Grid, Elsevier Ltd., 2003.

[20] J.F. Thompson, A. Warsi and C.W. Mastin, Numerical Grid Generation, Elsevier Science Publishing. 1985.

[21] C. A. J. Fletcher, Computational Techniques for Fluid Dynamics, Second Edition, Springer-Verlag Berlin Heidelberg, Germany, 1998,1991.

[22] I.Sezai, Modeling Solidification and Melting Using Curvilinear Moving Grids, unpublished report.

[23] F. Wolff, R. Viskanta, Solidification of a pure metal at a vertical wall in the presence of liquid superheat, Int. J. Heat Mass Transfer 31 (1988) 1735- 1744.

[24] C. Gau, R. Viskanta, Melting and solidification of a metal system in a rectangular cavity, Int. J. Heat Mass Transfer 27 (1984) 113-123.

[25] P.K. Khosla, S. Rubin, A diagonally dominant second-order accurate implicit scheme, Comput, Fluids 2 (1974) 207.

[26] B. Yu, W.Q. Tao, J.J. wei, Y. Kawaguchi, T. Tagawa, H. Ozoe, Discussion on momentum interpolation method for collocated grids of incompressible flow, Numerical Heat Transfer, Part B, 42 (2002) 141-166.

[27] C. M. Rhie and W. Chow, Numerical Study of Turbulent Flow Past an Airfoil with Trailing Edge Separation, AIAA J., vol. 21, pp. 1525-1532, 1983.

[28] S. Patankar and D. Spalding, A Calculation Procedure for Heat, Mass and Momentum Transfer in Three-Dimensional Parabolic Flows, Int. J. Heat Mass Transfer, vol. 15, pp. 1787-1806, 1972.

[29] N. Hannoun, V. Alexiadeas, and T. Mai, Resolving the Controversy over Tin and Gallium Melting in a Rectangular Cavity Heated from the side, Numer. Heat Transfer B, vol. 44, pp. 253-276, 2003.

[30] J. A. Dantzig, Modelting Liquid-Solid Phase Change with Melt Convection, Int. J. Numer. Meth. Eng., vol. 44, pp. 253-276, 2003.